Capturing the electron–electron cusp with the coupling-constant averaged exchange–correlation hole: A case study for Hooke's atoms

Lin Hou ; Tom J. P. Irons ; Yanyong Wang ; James W. Furness ; Andrew M. Wibowo-Teale ✉ ;
Jianwei Sun

Check for updates

View Online   Export Citation   CrossMark

Capturing the electron–electron cusp with the coupling-constant averaged exchange–correlation hole: A case study for Hooke's atoms

Lin Hou,[1] (ID) Tom J. P. Irons,[2,a)] (ID) Yanyong Wang,[1] (ID) James W. Furness,[1] (ID) Andrew M. Wibowo-Teale,[2,3,b)] (ID)
and Jianwei Sun[1,c)] (ID)

AFFILIATIONS

[1] Department of Physics and Engineering Physics, Tulane University, New Orleans, Louisiana 70118, USA

[2] School of Chemistry, University of Nottingham, University Park, Nottingham NG7 2RD, United Kingdom

[3] Hylleraas Centre for Quantum Molecular Sciences, Department of Chemistry, University of Oslo, P.O. Box 1033,
N-0315 Oslo, Norway

Note: This paper is part of the JCP Festschrift for John Perdew.
a)Electronic mail: tom.irons@nottingham.ac.uk
b)Author to whom correspondence should be addressed: andrew.teale@nottingham.ac.uk
c)Electronic mail: jsun@tulane.edu

ABSTRACT

In density-functional theory, the exchange–correlation (XC) energy can be defined exactly through the coupling-constant (λ) averaged XC hole $\bar{n}_{xc}(\mathbf{r}, \mathbf{r}')$, representing the probability depletion of finding an electron at $\mathbf{r}'$ due to an electron at $\mathbf{r}$. Accurate knowledge of $\bar{n}_{xc}(\mathbf{r}, \mathbf{r}')$ has been crucial for developing XC energy density-functional approximations and understanding their performance for molecules and materials. However, there are very few systems for which accurate XC holes have been calculated since this requires evaluating the one- and two-particle reduced density matrices for a reference wave function over a range of λ while the electron density remains fixed at the physical ($\lambda = 1$) density. Although the coupled-cluster singles and doubles (CCSD) method can yield exact results for a two-electron system in the complete basis set limit, it cannot capture the electron–electron cusp using finite basis sets. Focusing on Hooke's atom as a two-electron model system for which certain analytic solutions are known, we examine the effect of this cusp error on the XC hole calculated using CCSD. The Lieb functional is calculated at a range of coupling constants to determine the λ-integrated XC hole. Our results indicate that, for Hooke's atoms, the error introduced by the description of the electron–electron cusp using Gaussian basis sets at the CCSD level is negligible compared to the basis set incompleteness error. The system-, angle-, and coupling-constant-averaged XC holes are also calculated and provide a benchmark against which the Perdew–Burke–Ernzerhof and local density approximation XC hole models are assessed.

I. INTRODUCTION

Due to its relatively low computational scaling combined with high accuracy in the study of the electronic structure of many-body systems, density-functional theory (DFT) has become the most widely used electronic structure method with an increasing range of applications in condensed-matter physics, quantum chemistry, and materials science. In principle, DFT is an exact method with which the ground-state energy and electron density can be computed, from which many important physical and chemical properties can be extracted.[1] In practice, approximations must be introduced to DFT to make it computationally useful; in the Kohn–Sham formulation of DFT (KS-DFT),[2] the exchange–correlation (XC) component of the energy that carries the many-electron effects must be approximated.

Therefore, it is the quality of the XC approximation that determines the quality of a DFT calculation in predicting the total energy and other ground-state properties of interest.

An exact expression for the XC energy can be obtained in terms of the electron density $n(\mathbf{r})$ and the coupling-constant (λ) averaged XC hole density $\bar{n}_{xc}(\mathbf{r}, \mathbf{r}')$ via their Coulomb interaction[3] as

$$E_{xc}[n] = \frac{1}{2} \iint d\mathbf{r} \, d\mathbf{r}' \, \frac{n(\mathbf{r}) \bar{n}_{xc}(\mathbf{r}, \mathbf{r}')}{|\mathbf{r} - \mathbf{r}'|}, \quad (1)$$

where $\bar{n}_{xc}(\mathbf{r}, \mathbf{r}')$ is the probability depletion of finding an electron at $\mathbf{r}'$, given an electron located at $\mathbf{r}$. $\bar{n}_{xc}(\mathbf{r}, \mathbf{r}')$ is entirely attributed to quantum effects, which include the self-interaction correction, the Pauli exclusion principle (arising from the exchange symmetry of indistinguishable electrons), and the electron–electron correlation resulting from the Coulombic repulsion.[4] The first two effects give rise to the exchange hole density $n_x(\mathbf{r}, \mathbf{r}')$, which is completely negative and independent of the coupling constant. The remaining quantum effects produce the correlation hole, which is defined by subtracting the exchange hole density from $\bar{n}_{xc}(\mathbf{r}, \mathbf{r}')$ as $\bar{n}_c(\mathbf{r}, \mathbf{r}') = \bar{n}_{xc}(\mathbf{r}, \mathbf{r}') - n_x(\mathbf{r}, \mathbf{r}')$, yielding the λ-averaged correlation hole.

Equation (1) guarantees an accurate evaluation of the XC energy if an accurate XC hole model is provided. Therefore, the quality of XC hole models underpins the XC energy approximation and plays a fundamental role in understanding the quality and assessing the performance of a diverse range of density-functional approximations (DFAs) when applied to different systems and properties. However, practical DFT calculations only require approximations of the XC energy, leading to a tendency to neglect the importance of XC holes in favor of directly modeling the XC energy. This trend has led to relatively few XC-hole studies appearing in the literature. Notably, early successful DFAs such as the PW91 approximation of Perdew and Wang[5] were based on modeling the XC hole, and the construction of the strongly constrained and appropriately normed (SCAN) density functional was also grounded in the understanding of XC holes.[6] Recently, there have been new DFA developments based on XC holes.[7]

Although formally defined in Eq. (1), XC holes are challenging to evaluate accurately, contributing to the scarcity of XC hole studies. There are two significant challenges associated with this: (i) the XC hole has to be calculated for each coupling constant λ to evaluate the coupling-constant integrated XC hole; (ii) high-level electronic structure methods are required to obtain accurate ground-state wave functions for each λ. These methods typically have high-rank polynomial scaling with system size and become computationally intractable for large systems. The Lieb optimization approach[8] can address challenge (i) by transforming the problem of finding the ground-state electron density of a λ-interacting system into maximizing the Lieb functional of the λ-dependent external potential[9] while keeping the electron density fixed. In combination with the coupled-cluster singles and doubles method (CCSD), the Lieb optimization method has been applied to two-electron systems, such as the helium isoelectronic series, with a focus on the XC energy.[10,11] The CCSD method is exact in the complete basis set limit, equivalent to the full configuration interaction (FCI) approach for two-electron systems.

However, the λ-averaged XC hole has not been studied using the Lieb optimization with a CCSD reference wave function, even for simple two-electron systems. Therefore, it is currently not known how the basis set influences the quality of the calculated XC hole and the associated electron–electron cusp condition[12,13] of the correlation hole[14] when the coupling-constant averaged quantities are considered. The electron–electron cusp condition describes the behavior of a many-electron wave function when two spin anti-parallel electrons come infinitesimally close to each other, arising due to the singularity of the Coulomb repulsion at the coalescence point. This dynamical correlation effect at zero separation introduces non-smoothness into the many-body wave function, which cannot be effectively represented by orbital product expansion wave functions.[15] Increasing the basis set size can help reduce the cusp error, but this approach is limited by the unfavorable computational scaling of high-level electronic structure methods.

In this study, we examine the electron–electron cusp condition and basis set effects on the XC hole through the calculation of the Lieb functional at the CCSD level for a simple model system, namely Hooke's atom (Hookium). By introducing the harmonic-oscillator potential as the external potential in the Hamiltonian of a two-electron system, given in atomic units as

$$\hat{H} = -\frac{1}{2}\nabla_1^2 + \frac{1}{2}k\mathbf{r}_1^2 - \frac{1}{2}\nabla_2^2 + \frac{1}{2}k\mathbf{r}_2^2 + \frac{1}{|\mathbf{r}_1 - \mathbf{r}_2|}, \quad (2)$$

the resulting problem is one of the few examples of a two-electron system for which a series of exact solutions exist—in this case, an infinite set of solutions corresponding to different harmonic confinement constants, k.[16,17] The Hookium atom is, therefore, a useful reference for evaluating XC hole models since the exact XC holes can be computed.

We commence in Sec. II by providing an overview of the theoretical framework for computing the λ-dependent XC hole, the Lieb optimization method, the electron–electron cusp condition in Coulombic systems, and the solvable Hookium model. Computational details are then discussed in Sec. III. In Sec. IV, we examine the basis set effects and cusp condition effects on the XC hole calculated at the CCSD level at $\lambda = 1$ (the physical system), for which the exact wave function solution is known. We then compare and benchmark the local density approximation (LDA) and Perdew–Burke–Ernzerhof (PBE) XC hole models with the coupling-constant averaged XC hole from Lieb optimizations at the CCSD level. System- and angle-averaged XC holes are calculated to enable direct comparison between the benchmark data and these simple density-functional models. Finally, we conclude our work with a brief summary in Sec. V.

II. THEORY AND METHODOLOGY

A. The exchange–correlation hole and the coupling constant

In KS-DFT, the ground-state energy of a many-electron system in an external potential $v_{ext}(\mathbf{r})$ is obtained by mapping the interacting system of electrons to an auxiliary non-interacting system of electrons with the same electron density. The Schrödinger equation for this auxiliary system can then be solved in a basis of one-electron orbitals.[2] The ground-state electronic energy is thus expressed as a

functional of the electron density $n(\mathbf{r})$, which can be resolved into the sum of several contributions as

$$E[n] = T_s[n] + E_H[n] + E_{xc}[n] + \int d\mathbf{r}\, v_{ext}(\mathbf{r}) n(\mathbf{r}), \quad (3)$$

where T_s is the non-interacting kinetic energy, which is evaluated exactly using the KS orbitals, and E_H is the classical electrostatic Hartree energy, which is evaluated exactly in terms of $n(\mathbf{r})$. The only term in Eq. (3) that must be approximated is the XC energy $E_{xc}[n]$, which describes all of the many electron effects in the system.

The KS non-interacting system may be linked to the physically interacting system by continuously varying the strength of the electron–electron interaction between the non-interacting and physically interacting limits by scaling the two-electron operator $\hat{V}_{ee}$ by a coupling constant λ between zero and one. The electronic state evolves through a family of solutions to the λ-interacting Hamiltonian,

$$\hat{H}_\lambda = \hat{T} + \lambda \hat{V}_{ee} + \sum_i v_\lambda(\mathbf{r}_i), \quad (4)$$

where $\hat{T}$ is the kinetic energy operator and v_λ is a modified external potential, thus establishing an adiabatic connection between the non-interacting and physically interacting systems.[18] The modified external potential v_λ is determined for each interaction strength such that the density remains constant at the physical ($\lambda = 1$) density for all λ. Clearly, v_λ reduces to the local KS potential v_s when $\lambda = 0$ and is equal to the physical external potential v_{ext} when $\lambda = 1$.

Supposing Ψ_λ is the non-degenerate normalized ground-state many-electron wave function of the λ-interacting system with N electrons, the diagonal part of the second-order reduced density matrix is expressed as[13,19]

$$n_2^\lambda(\mathbf{r}, \mathbf{r}') \equiv N(N-1) \sum_{\sigma_1, \ldots, \sigma_N} \int d\mathbf{r}_3 \cdots \int d\mathbf{r}_N$$
$$\times \left| \Psi_\lambda(\mathbf{r}\sigma_1, \mathbf{r}'\sigma_2, \mathbf{r}_3\sigma_3, \ldots, \mathbf{r}_N\sigma_N) \right|^2. \quad (5)$$

This two-particle density may be used to evaluate the expectation value of two-body operators,[4] but it cannot be diagonalized by a unitary transformation of one-electron basis functions.[13] The XC hole density at each coupling strength λ is defined as

$$n_{xc}^\lambda(\mathbf{r}, \mathbf{r}') = \frac{n_2^\lambda(\mathbf{r}, \mathbf{r}')}{n(\mathbf{r})} - n(\mathbf{r}'), \quad (6)$$

where the second term removes the classical Hartree contribution to the two-particle density $n(\mathbf{r})n(\mathbf{r}')$, with the remaining $n_{xc}^\lambda(\mathbf{r}, \mathbf{r}')$ accounting for only the XC effects. The λ-averaged XC hole density is given by coupling constant integration over this quantity,

$$\bar{n}_{xc}(\mathbf{r}, \mathbf{r}') = \int_0^1 d\lambda\, n_{xc}^\lambda(\mathbf{r}, \mathbf{r}'), \quad (7)$$

from which an exact expression for E_{xc} can be obtained, shown in Eq. (1).

At $\lambda = 0$, the XC hole is reduced to the exchange hole,

$$n_x(\mathbf{r}, \mathbf{r}') = n_{xc}^{\lambda=0}(\mathbf{r}, \mathbf{r}')$$
$$= -\frac{\sum_\sigma \sum_{i,j}^{occ} \psi_{i\sigma}^*(\mathbf{r}) \psi_{j\sigma}(\mathbf{r}) \psi_{j\sigma}^*(\mathbf{r}') \psi_{i\sigma}(\mathbf{r}')}{n(\mathbf{r})}, \quad (8)$$

where $\psi_{i\sigma}(\mathbf{r})$ are the KS spin-orbitals. Therefore, the λ-averaged correlation hole can be defined by

$$\bar{n}_{xc}(\mathbf{r}, \mathbf{r}') = n_x(\mathbf{r}, \mathbf{r}') + \bar{n}_c(\mathbf{r}, \mathbf{r}'). \quad (9)$$

Furthermore, since the Coulomb operator has spherical symmetry, the XC energy may be computed *exactly* from the spherically averaged XC hole. As a result, the system- and spherically averaged XC hole density $\langle \bar{n}_{xc} \rangle(u)$ is a useful quantity that can be modeled in order to construct XC energy functionals. This may be written in terms of the distance vector $\mathbf{u} = \mathbf{r}' - \mathbf{r}$ as

$$\langle \bar{n}_{xc} \rangle(u) = \frac{1}{N} \int d\mathbf{r}\, n(\mathbf{r}) \int \frac{d\Omega_{\mathbf{u}}}{4\pi} \bar{n}_{xc}(\mathbf{r}, \mathbf{r} + \mathbf{u}), \quad (10)$$

where $\Omega_{\mathbf{u}}$ is the solid angle around direction $\mathbf{u}$, and integration is carried out to average over this angle and the spatial coordinates of the entire system. It is a remarkable result that the XC energy may then be expressed precisely as a one-dimensional integral over $u = |\mathbf{r}' - \mathbf{r}|$ for any system,

$$E_{xc}[n] = \frac{N}{2} \int_0^\infty du\, 4\pi u^2 \frac{\langle \bar{n}_{xc} \rangle(u)}{u}, \quad (11)$$

$$= \frac{N}{2} \int_0^\infty du\, \varepsilon_{xc}(u), \quad (12)$$

where we identify $\varepsilon_{xc}(u) = 4\pi u \langle \bar{n}_{xc} \rangle(u)$. The exact system- and spherically averaged exchange and correlation holes satisfy the following sum rules, respectively,

$$\int_0^\infty du\, 4\pi u^2 \langle n_x \rangle(u) = -1, \quad (13)$$

$$\int_0^\infty du\, 4\pi u^2 \langle \bar{n}_c \rangle(u) = 0. \quad (14)$$

B. The Lieb optimization

Given a Hamiltonian $\hat{H}_\lambda[v_\lambda]$, the ground-state energy $E_\lambda[v_\lambda]$ for an N-electron system is given by the Rayleigh–Ritz variation principle as

$$E_\lambda[v_\lambda] = \inf_{\Psi_\lambda \in \mathscr{W}_N} \langle \Psi_\lambda | \hat{H}_\lambda[v_\lambda] | \Psi_\lambda \rangle, \quad (15)$$

where $\mathscr{W}_N$ is the set of all L^2-normalized, antisymmetric N-electron wave functions with a finite kinetic energy. The ground-state energy in Eq. (15) is well-defined for all potentials $v_\lambda \in \chi^*$ with $\chi^* = L^{\frac{3}{2}} + L^\infty$, a vector space containing all Coulomb potentials. For a variationally determined solution to Eq. (15), $E_\lambda[v_\lambda]$ is concave and continuous in v_λ.

Following the convex-conjugate formulation of DFT by Lieb,[9] the universal density functional $F_\lambda[n]$ may be defined as the

Legendre–Fenchel transform of the ground-state energy of Eq. (15) as

$$F_\lambda[n] = \sup_{v_\lambda \in \chi^*} \left[E_\lambda[v_\lambda] - \int d\mathbf{r}\, n(\mathbf{r}) v_\lambda(\mathbf{r}) \right], \qquad (16)$$

which is convex in n by construction and thus may be defined not only for the exact $E_\lambda[v_\lambda]$ but also used for any approximate (even non-concave) model $E_\lambda[v_\lambda]$ (see Ref. 11 for further discussion). The Legendre–Fenchel transformation of $F_\lambda[n]$ as defined in Eq. (16) yields an expression for the Hohenberg–Kohn variation principle

$$E_\lambda^*[v_\lambda] = \inf_{n \in \chi} \left[F_\lambda[n] + \int d\mathbf{r}\, n(\mathbf{r}) v_\lambda(\mathbf{r}) \right], \qquad (17)$$

in which the biconjugate functional $E_\lambda^*[v_\lambda]$ is the concave envelope to $E_\lambda[v_\lambda]$ such that $E_\lambda^*[v_\lambda] \geq E_\lambda[v_\lambda]$ and $\chi = L^3 \cap L^1$ is the space encompassing all N-representable densities and to which χ^* is the dual vector space. The conjugate functionals Eq. (16) and Eq. (17) are related by Fenchel's inequality as

$$F_\lambda[n] \geq E_\lambda^*[v_\lambda] - \int d\mathbf{r}\, n(\mathbf{r}) v_\lambda(\mathbf{r}) \quad \forall n \in \chi, \, v_\lambda \in \chi^*, \qquad (18)$$

which becomes an equality by maximization of the right-hand side with respect to v_λ which, for non-degenerate solutions, is the same as satisfying the stationary condition

$$\frac{\delta E_\lambda^*[v_\lambda]}{\delta v_\lambda(\mathbf{r})} = n(\mathbf{r}). \qquad (19)$$

By definition, $E_\lambda^*[v_\lambda]$ is concave in v_λ and hence has no more than one stationary point; if a solution to Eq. (19) exists, it is, therefore, unique. This can also be expressed by rearranging Eq. (18) to the form $E_\lambda^*[v_\lambda] \leq F_\lambda[n] + \int d\mathbf{r}\, n(\mathbf{r}) v_\lambda(\mathbf{r})$, which becomes an equality by minimization of the right-hand side with respect to $n(\mathbf{r})$, thus satisfying the stationary condition

$$\frac{\delta F_\lambda[n]}{\delta n(\mathbf{r})} = -v_\lambda(\mathbf{r}), \qquad (20)$$

where v_λ is the optimizing potential. In the Lieb optimization method, the universal density functional F_λ is maximized with respect to the potential $v_\lambda(\mathbf{r})$ for a given electronic structure method with energy functional E_λ and yielding density $n(\mathbf{r})$. To construct the density-fixed adiabatic connection, the optimizing potential $v_\lambda(\mathbf{r})$ is that for which E_λ yields the physically interacting $\lambda = 1$ density for all values of $\lambda \in [0,1]$.[10,11] In fact, the relation in Eq. (20) is problematic since the exact functional has been shown to be discontinuous and not differentiable.[20] However, differentiability can be restored by regularization of F_λ, which can be achieved via Moreau–Yosida regularization[21] or in practical calculations by the closely related smoothing-norm procedure of Heaton-Burgess et al.,[22] the latter being employed in the present work.

The universal density functional F_λ may be written as a sum of terms according to the Kohn–Sham decomposition as[2]

$$F_\lambda[n] = T_s[n] + \lambda E_H[n] + \lambda E_x[n] + E_{c,\lambda}[n], \qquad (21)$$

in which T_s is the non-interacting kinetic energy, E_H is the classical Coulomb energy, E_x is the exchange energy, and $E_{c,\lambda}$ is the

λ-interacting correlation energy. Substituting Eq. (21) into Eq. (20) yields an expression for the optimizing potential in terms of its individual contributions,

$$\frac{\delta F_\lambda[n]}{\delta n(\mathbf{r})} = \frac{\delta T_s[n]}{\delta n(\mathbf{r})} + \lambda \frac{\delta E_H[n]}{\delta n(\mathbf{r})} + \lambda \frac{\delta E_x[n]}{\delta n(\mathbf{r})} + \frac{\delta E_{c,\lambda}[n]}{\delta n(\mathbf{r})},$$
$$-v_\lambda(\mathbf{r}) = -v_s(\mathbf{r}) + \lambda v_H(\mathbf{r}) + \lambda v_x(\mathbf{r}) + v_{c,\lambda}(\mathbf{r}). \qquad (22)$$

Identifying that $v_{\lambda=1} = v_{ext}$, the external potential due to the electrostatic potential of the nuclei, and $v_{\lambda=0} = v_s$, the Kohn–Sham potential may be eliminated from Eq. (22) to yield the expression for the optimizing potential at interaction strength λ as

$$v_\lambda(\mathbf{r}) = v_{ext}(\mathbf{r}) + (1-\lambda) v_H(\mathbf{r}) + (1-\lambda) v_x(\mathbf{r}) + [v_{c,1}(\mathbf{r}) - v_{c,\lambda}(\mathbf{r})]. \qquad (23)$$

In order to optimize F_λ with respect to the potential, it is expanded in a Gaussian basis, as proposed by Wu and Yang,[8,23]

$$v_{\lambda,\mathbf{b}}(\mathbf{r}) = v_{ext}(\mathbf{r}) + (1-\lambda) v_H(\mathbf{r}) + (1-\lambda) v_{ref}(\mathbf{r}) + \sum_t b_t g_t(\mathbf{r}), \qquad (24)$$

in which v_H is the Coulomb potential evaluated with an input $\lambda = 1$ density n_{in}, v_{ref} is a reference exchange potential also evaluated on this density to ensure that v_λ has the correct asymptotic behavior, and g_t is a set of Gaussian functions with expansion coefficients b_t. The form of the reference potential employed in this work is that of a localized Hartree–Fock potential,[24] corrected at long-range by an approximate Fukui potential.[25] The details of the construction of the reference potential are given in the Appendix.

With the parameterization of the potential in Eq. (24), the Lieb functional can be defined as an optimization of the objective function,

$$G_{\lambda,n}[\mathbf{b}] = E_\lambda[v_{\lambda,\mathbf{b}}] - \int d\mathbf{r}\, n(\mathbf{r}) v_{\lambda,\mathbf{b}}(\mathbf{r}), \qquad (25)$$

with respect to variations in the potential basis coefficients $\mathbf{b}$; the gradient of Eq. (25) with respect to the potential basis coefficients is given by

$$\frac{\partial G_{\lambda,n}[\mathbf{b}]}{\partial b_t} = \int d\mathbf{r}\, [n_{\lambda,\mathbf{b}}(\mathbf{r}) - n_{in}(\mathbf{r})] g_t(\mathbf{r}), \qquad (26)$$

while the second derivative of the objective function with respect to the potential basis coefficients is given by

$$\frac{\partial^2 G_{\lambda,n}[\mathbf{b}]}{\partial b_t \partial b_u} = \iint d\mathbf{r}\, d\mathbf{r}'\, g_t(\mathbf{r}) g_u(\mathbf{r}') \frac{\delta n_{\lambda,\mathbf{b}}(\mathbf{r})}{\delta v_{\lambda,\mathbf{b}}(\mathbf{r}')}. \qquad (27)$$

It can be seen from Eq. (26) that the stationary condition of Eq. (19) will be satisfied when the iterating density $n_{\lambda,\mathbf{b}}$ becomes equal to the input density n_{in}. In this work, the objective function is optimized by an approximate Newton approach implemented in the QUEST program;[26] this is a second-order optimization algorithm in which the Hessian is approximated by the non-interacting Hessian, given by Eq. (27) at $\lambda = 0$.[27] In this process, the potential basis coefficients are updated at each iteration using a backtracking line-search, and the wave function is evaluated with the corresponding potential $v_{\lambda,\mathbf{b}}$, yielding the energy E_λ and iterating density $n_{\lambda,\mathbf{b}}$ from which the

objective function Eq. (25), gradient Eq. (26), and approximate Hessian are constructed. At the point of convergence, for which Eq. (26) becomes zero, the optimizing potential may be used to obtain the λ-interacting one- and two-particle reduced density matrices required for the construction of the λ-interacting XC hole as described in Sec. II A. With the above calculations completed for each λ, a series of λ-dependent and then λ-averaged quantities such as the XC holes and XC energies given in Eqs. (5)–(11) can be readily obtained.

C. The electron–electron cusp condition

For a Coulombic system, the electron–electron cusp condition describes the behavior of the electrons in exact eigenfunctions of the Schrödinger equation, which exhibit a cusp at the points of electron coalescence due to singularities in the Coulomb potential at such points.[28] The exact electron–electron cusp condition may be expressed using the spherically averaged XC hole, $n_{xc}^{\lambda}(\mathbf{r}, u) = \int \frac{d\Omega_u}{4\pi} n_{xc}^{\lambda}(\mathbf{r}, \mathbf{r} + \mathbf{u})$, as[29]

$$n_{xc}^{\lambda\prime}(\mathbf{r}, 0) = \left.\frac{\partial n_{xc}^{\lambda}(\mathbf{r}, u)}{\partial u}\right|_{u \to 0^+} = \lambda\left[n_{xc}^{\lambda}(\mathbf{r}, 0) + n(\mathbf{r})\right]. \quad (28)$$

The electron cusp condition may be written in terms of the system and spherically averaged XC hole defined in Sec. II A as

$$\langle n_{xc}^{\lambda\prime}\rangle(0) = \frac{1}{N}\int d\mathbf{r}\, n(\mathbf{r}) \left.\frac{\partial n_{xc}^{\lambda}(\mathbf{r}, u)}{\partial u}\right|_{u \to 0^+}, \quad (29)$$

the substitution of Eq. (28) into which yields

$$\langle n_{xc}^{\lambda\prime}\rangle(0) = \lambda\left[\frac{1}{N}\int d\mathbf{r}\, n(\mathbf{r}) n_{xc}^{\lambda}(\mathbf{r}, 0) + \frac{1}{N}\int d\mathbf{r}\, n^2(\mathbf{r})\right]$$
$$= \lambda\left[\langle n_{xc}^{\lambda}\rangle(0) + \frac{1}{N}\int d\mathbf{r}\, n^2(\mathbf{r})\right]. \quad (30)$$

The electronic cusp condition may be written in terms of the system and spherically averaged correlation hole by resolving the on-top XC hole into exchange and correlation components, then inserting the identity for the on-top exchange hole for a spin-unpolarized system, $n_x(\mathbf{r}, 0) = -n(\mathbf{r})/2$, yielding

$$\langle n_{xc}^{\lambda\prime}\rangle(0) = \lambda\left[\frac{1}{N}\int d\mathbf{r}\, n(\mathbf{r}) n_c^{\lambda}(\mathbf{r}, 0) + \frac{1}{2N}\int d\mathbf{r}\, n^2(\mathbf{r})\right]$$
$$= \lambda\left[\langle n_c^{\lambda}\rangle(0) + \frac{1}{2N}\int d\mathbf{r}\, n^2(\mathbf{r})\right] = \langle n_c^{\lambda\prime}\rangle(0). \quad (31)$$

The final identity in Eq. (31) follows from the Pauli principle, a corollary of which is that the cusp condition only arises between electrons with anti-parallel spin and is thus exclusively a correlation effect.

D. Hookium atoms

A Hookium atom is a model system comprising two electrons confined by a harmonic potential rather than a Coulomb potential,[16] with the electronic Hamiltonian given in Eq. (2). Introducing the center of mass coordinate $\mathbf{R} = (\mathbf{r}_1 + \mathbf{r}_2)/2$ and the relative separation

vector $\mathbf{u} = \mathbf{r}_1 - \mathbf{r}_2$, the Hookium atom Hamiltonian may be resolved into a center of mass and relative separation term as

$$\hat{H} = \underbrace{\left(-\frac{1}{4}\nabla_{\mathbf{R}}^2 + k\mathbf{R}^2\right)}_{\hat{H}(\mathbf{R})} + \underbrace{\left(-\nabla_{\mathbf{u}}^2 + \frac{1}{4}k\mathbf{u}^2 + \frac{1}{u}\right)}_{\hat{H}(\mathbf{u})}. \quad (32)$$

The second term $\hat{H}(\mathbf{u})$ is of particular interest as it describes the relative motion between the two interacting electrons bound by the harmonic potential and is effectively a one-body problem with Schrödinger equation $\hat{H}(\mathbf{u})\varphi(\mathbf{u}) = \varepsilon\varphi(\mathbf{u})$. Using a separation of variables to write $\varphi(\mathbf{u})$ in terms of the product of radial and angular components

$$\varphi(\mathbf{u}) = \frac{g(u)}{u} Y_{lm}, \quad g(u) = \exp\left(-\sqrt{k}u^2/4\right) T(u), \quad (33)$$

where Y_{lm} is the spherical harmonic function describing the angular wave function, a second-order differential equation for $T(u)$ can be obtained. By inserting the regular solution

$$T(u) = u\sum_{i=0}^{\infty} a_i u^i, \quad (34)$$

into the differential equation, a recurrence relation[16] can be found for the coefficients $\{a_i, i \geq 2\}$,

$$a_{i+1} = \frac{a_i + \left[(i + 1/2)\sqrt{k} - \varepsilon\right]a_{i-1}}{(i+1)(i+2)}, \quad (35)$$

where we only consider the ground state with the angular momentum $l = 0$. A series of exact solutions can be determined by imposing the condition $a_M = a_{M+1} = 0$, leading to $a_i = 0$ for all $i \geq M$. Consequently, M represents the polynomial order of $T(u)$ in the radial wave function $\varphi(u)$. For further details of the exact solutions and derived quantities used as a benchmark in this work, the reader is referred to Ref. 16.

For the ground state with $l = 0$, M is roughly proportional to $k^{-7.9}$, as observed by fitting the values of M against k.[16] Since k is the harmonic constant that determines the strength with which electrons are confined, an increase in M implies less confinement and a more radially diffuse electron density.

However, it is obvious that there does not exist an analytical wave function solution for the Hookium atom with the electron–electron interaction scaled by an arbitrary $\lambda \neq 1$. Therefore, the coupling-constant-averaged correlation hole for the Hookium atom has seldom been studied, and only the correlation hole at $\lambda = 1$ has been comprehensively studied[30] and used to benchmark correlation hole models.[31–33]

For example, the exchange hole and the correlation hole of the Hookium atom with $k = 1/4$ (corresponding to $M = 2$) for the $\lambda = 1$ case have been carefully studied in Ref. 30, which is also used to benchmark the system- and angle-averaged XC hole models of different *meta*-GGAs.[31] Using only the $\lambda = 1$ results, the validity of the electronic cusp condition in the ground state of the Hookium atom for arbitrary harmonic confinement k has been demonstrated,[32] and it has been demonstrated that the LDA hole model can precisely capture the cusp condition of the Hookium atom.[33]

24 January 2024 15:35:23

In this work, we employ the exact solutions of the Hookium atom at $\lambda = 1$ to benchmark those calculated from the CCSD wave function. We then use the Lieb optimization with a CCSD wave function to calculate λ-averaged XC holes for the Hookium atom, which can serve as a benchmark for XC hole models.

III. COMPUTATIONAL DETAILS

In this work, all calculations are carried out using the QUEST program[26] with the spin-restricted CCSD wave function as the reference method. The convergence of self-consistent field calculations was accelerated using the C1-DIIS method, with a convergence threshold of 10^{-12} a.u. on the norm of the DIIS error vector. For the CCSD calculations, the convergence threshold for both the excitation amplitudes and de-excitation amplitudes required for evaluation of the CCSD one- and two-particle densities was 10^{-10} a.u. for the norm of the difference of the amplitudes between iterations.

Lieb optimizations were carried out at the CCSD level for a range of interaction strengths $\lambda \in [0, 1]$ using the approximate Newton method described in Sec. II B. In each case, the CCSD $\lambda = 1$ density was used as input to the Lieb functional in order to fix the density along the adiabatic connection at its physical value. The potential was regularized using the smoothing norm method[22] with a regularization parameter of 10^{-5} a.u. The convergence of the Lieb optimization was based on the norm of the gradient with respect to potential expansion coefficients, with a convergence threshold of 10^{-8} a.u. used throughout. To improve convergence, a slightly smaller basis set was used for the potential expansion than was used for the orbital expansion. In this work, a series of Dunning basis sets were employed, with the orbital basis sets Y-aug-cc-pVXZ (Y = d, t, q, p, s; X = D, T, Q, 5, 6) and the corresponding potential basis sets of $(Y-1)$-aug-cc-pVXZ ($Y-1$ = d, t, q, p; X = D, T, Q, 5, 6).[34–36] In each case, the basis sets were uncontracted spherical Gaussians with exponents for the helium atom used throughout.

To evaluate the system- and spherically averaged XC holes, a nested numerical quadrature was employed. The spherically averaged XC hole n_{xc}^λ was constructed by angular integration using an order-41 Lebedev quadrature grid at each reference point,[37,38] leading to

$$n_{xc}^\lambda(\mathbf{r}, u) = \frac{1}{4\pi} \int d\Omega_{\mathbf{u}} n_{xc}^\lambda(\mathbf{r}, \mathbf{r} + \mathbf{u})$$
$$\approx \sum_i^{N_\Omega} w_i^\Omega n_{xc}^\lambda(\mathbf{r}, \mathbf{r}_i^\Omega), \qquad (36)$$

with quadrature weights w_i^Ω and nodes $\mathbf{r}_i^\Omega$ associated with the angular quadrature nodes (φ_i, θ_i) by

$$x_i^\Omega = u \cos\varphi_i \sin\theta_i + x,$$
$$y_i^\Omega = u \sin\varphi_i \sin\theta_i + y,$$
$$z_i^\Omega = u \cos\theta_i + z,$$

with $\mathbf{r} = (x, y, z)$ and $\mathbf{r}_i^\Omega = (x_i^\Omega, y_i^\Omega, z_i^\Omega)$. The Lebedev integration order was selected to recover the sum rules of Eqs. (13) and (14) to better than 10^{-5}.

The system-averaging was then carried-out by numerical integration of the reference point using a full quadrature grid, with the angular component again given by the order-41 Lebedev quadrature and radial component constructed using the scheme of Lindh, Malmqvist, and Gagliardi[39] with a relative error threshold of 10^{-10} a.u.,

$$\langle n_{xc}^\lambda \rangle(u) = \frac{1}{N} \int d\mathbf{r}\, n(\mathbf{r}) n_{xc}^\lambda(\mathbf{r}, u)$$
$$\approx \sum_i^{N_r} \sum_j^{N_\Omega} w_i^r w_j^\Omega n(\mathbf{r}_{ij}) n_{xc}^\lambda(\mathbf{r}_{ij}, u), \qquad (37)$$

where w_i^r is the weight of the radial quadrature and $\mathbf{r}_{ij}$ is the product of radial quadrature nodes $\mathbf{r}_i^r$ and angular quadrature nodes $\mathbf{r}_j^\Omega$.

Exact analytical results for the Hookium atom at $\lambda = 1$, as described in Sec. II D, were also calculated with Mathematica,[40] allowing us to carefully assess the accuracy of the finite basis CCSD calculations.

IV. RESULTS AND DISCUSSION

A. Accuracy of finite-basis CCSD Hookium solutions

As described in Sec. II B, $n(\mathbf{r})$ given by CCSD is used as the reference electron density of the physical interacting system for the Lieb optimization in Eq. (25). Therefore, we first assess the quality of CCSD calculated total energies and densities with a range of orbital basis set sizes for Hookium by comparing them with the exact analytical results.

1. Total energies

Table I lists the percentage errors (PEs) for the finite-basis CCSD total energies with respect to the exact results for different solutions to the Hookium atom labeled by M, as described in Sec. II D, computed with different basis sets. All PEs are positive, as expected since CCSD is equivalent to FCI for these two-electron systems, and so the energy approaches the complete basis set FCI energy from above. In general, the accuracy of the energies can be improved systematically by using basis sets with a higher cardinal number X or a higher augmentation with diffuse functions Y. This leads to a reduction in the PEs to be in the range of 0.2%–2.5%. It is clear that, for the solutions with $M < 5$, PEs below 1% can be achieved with triply augmented basis sets with cardinal numbers of 4 or above. Indeed, adding extra diffuse functions does not further improve the accuracy of the results for these solutions. However, for larger values of M, it is essential to include many more diffuse functions to obtain reasonable accuracy. For $5 \le M \le 8$, pentuple augmentation is required to achieve PEs below 2%, and for $M > 8$, hextuple augmentation is required. The dependence on the cardinal number X is less significant; once sufficient diffuse functions are included for a given value of M, there appears to be little benefit in using basis sets with $X > 4$.

2. Electron densities

In Fig. 1, we plot the CCSD electron densities of Hookium atom solutions with $2 \le M \le 5$ radially from the atomic nucleus. For comparison, the densities of the corresponding exact solutions are also shown. The convergence of CCSD electron densities at each Hookium solution M is examined by gradually increasing the size of the

TABLE I. Percentage errors of the CCSD total energy E_{tot}^{CCSD} relative to the exact results for the Hookium atom solutions with $M = 2$–11. Orbital basis sets of Y-aug-cc-pVXZ (X = D, T, Q, 5, 6; Y = d, t, q, p, s) are employed.

Orbital basis	$M = 2$	$M = 3$	$M = 4$	$M = 5$	$M = 6$	$M = 7$	$M = 8$	$M = 9$	$M = 10$	$M = 11$
d-aug-cc-pVDZ	1.9%	4.5%	8.6%	53.6%	129.1%	228.1%	348.5%	489.6%	651.0%	832.6%
d-aug-cc-pVTZ	0.2%	1.4%	6.5%	34.9%	93.5%	173.8%	272.6%	388.9%	522.3%	672.5%
d-aug-cc-pVQZ	0.4%	0.8%	5.6%	33.0%	90.2%	168.8%	265.7%	379.7%	510.5%	657.9%
d-aug-cc-pV5Z	0.5%	0.6%	4.7%	32.7%	90.1%	168.8%	265.7%	379.8%	510.7%	658.1%
d-aug-cc-pV6Z	0.3%	0.3%	4.6%	34.5%	93.6%	174.2%	273.3%	389.8%	523.5%	674.0%
t-aug-cc-pVDZ	1.9%	3.8%	4.2%	2.0%	11.9%	40.2%	81.8%	133.8%	194.9%	264.5%
t-aug-cc-pVTZ	0.2%	1.3%	0.6%	6.5%	14.0%	35.3%	70.4%	116.2%	170.9%	233.8%
t-aug-cc-pVQZ	0.4%	0.8%	0.5%	5.7%	14.1%	36.8%	73.2%	120.2%	176.3%	240.6%
t-aug-cc-pV5Z	0.5%	0.5%	0.5%	4.3%	14.0%	39.3%	78.1%	127.5%	186.0%	253.0%
t-aug-cc-pV6Z	0.3%	0.2%	0.4%	3.8%	17.5%	48.3%	92.6%	147.7%	212.5%	286.3%
q-aug-cc-pVDZ	1.9%	3.7%	3.9%	1.5%	6.0%	3.3%	3.5%	13.4%	31.1%	54.7%
q-aug-cc-pVTZ	0.2%	1.3%	0.5%	3.6%	0.7%	6.6%	14.0%	24.8%	41.5%	64.5%
q-aug-cc-pVQZ	0.4%	0.7%	0.4%	2.8%	0.9%	7.2%	15.1%	27.5%	46.5%	71.9%
q-aug-cc-pV5Z	0.5%	0.5%	0.4%	1.9%	1.4%	6.2%	14.7%	30.0%	52.4%	81.0%
q-aug-cc-pV6Z	0.3%	0.2%	0.3%	0.8%	1.7%	7.1%	20.0%	41.5%	70.5%	105.7%
p-aug-cc-pVDZ	1.9%	3.7%	3.9%	1.4%	5.7%	2.7%	3.0%	7.8%	6.1%	3.6%
p-aug-cc-pVTZ	0.2%	1.3%	0.5%	3.4%	0.7%	4.2%	1.7%	1.3%	6.8%	14.4%
p-aug-cc-pVQZ	0.4%	0.7%	0.3%	2.5%	0.7%	3.2%	1.0%	3.3%	10.3%	18.1%
p-aug-cc-pV5Z	0.5%	0.5%	0.4%	1.7%	1.1%	2.3%	1.3%	4.4%	10.3%	18.6%
p-aug-cc-pV6Z	0.3%	0.2%	0.3%	0.6%	1.2%	0.9%	1.7%	6.0%	14.4%	27.2%
s-aug-cc-pVDZ	1.9%	3.7%	3.9%	1.4%	5.6%	2.7%	2.9%	7.3%	5.6%	3.4%
s-aug-cc-pVTZ	0.2%	1.3%	0.5%	3.4%	0.6%	4.0%	1.5%	1.2%	4.5%	3.5%
s-aug-cc-pVQZ	0.4%	0.7%	0.3%	2.5%	0.7%	2.9%	0.7%	2.2%	3.3%	1.8%
s-aug-cc-pV5Z	0.5%	0.5%	0.4%	1.6%	1.0%	2.0%	0.7%	2.4%	2.5%	2.1%
s-aug-cc-pV6Z	0.3%	0.2%	0.3%	0.6%	1.1%	0.6%	1.2%	1.6%	1.0%	2.5%

t-aug-cc-pVXZ basis set by changing the cardinal number X from 2 to 6.

Figure 1 shows that, as the order of the Hookium solution M increases from 2 to 5, the corresponding electron density becomes increasingly spatially diffuse. Interestingly, the convergence behavior of the density with respect to the basis set appears to be dependent on whether the value of M is even or odd. Specifically, for the $M = 2$ and $M = 4$ solutions, the CCSD densities converge to the corresponding exact densities relatively quickly with increasing basis set size, and there is no discernible difference in the results obtained with basis sets with $X \geq 3$. However, convergence of the density with respect to the basis set is considerably slower for the $M = 3$ and $M = 5$ solutions. It should be noted that, for $M = 5$, the CCSD energies and densities in the largest basis set t-aug-cc-pV6Z both have a greater error than those from the smallest basis set t-aug-cc-pVDZ considered here, as can be seen in Table I. This indicates that for
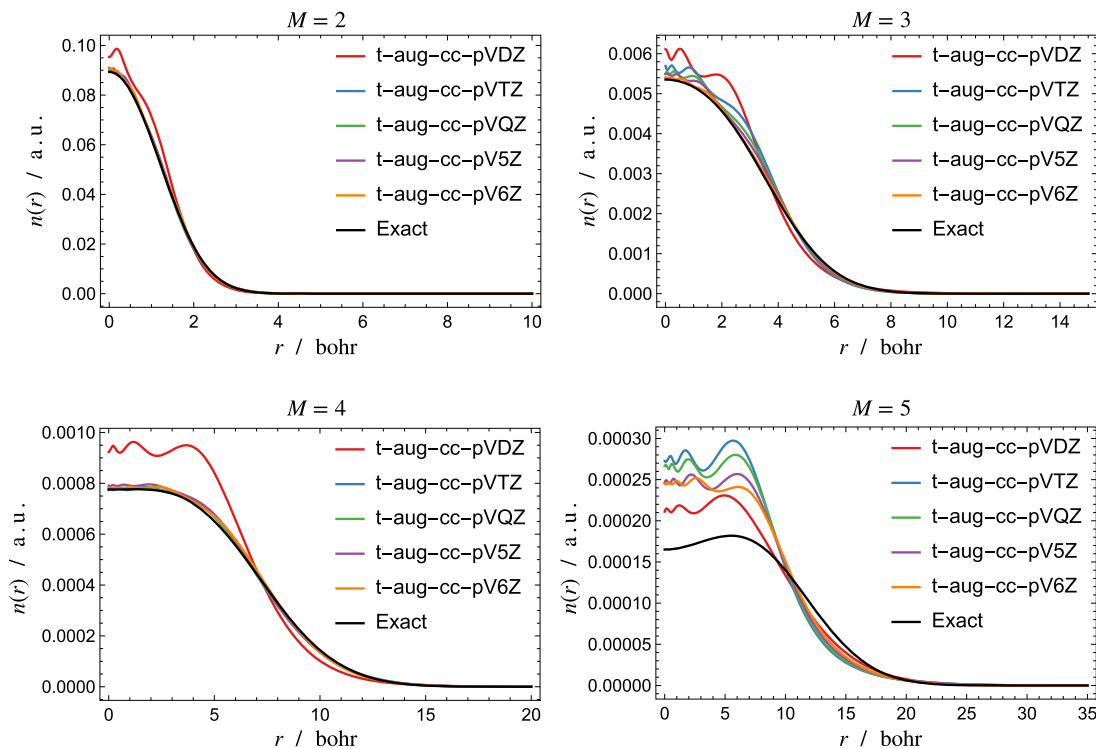
FIG. 1. Radial electron densities calculated from CCSD for Hookium solutions with $M = 2, 3, 4, 5$, where orbital basis sets with t-aug-cc-pVXZ (X = D, T, Q, 5, 6) are employed.

$M = 5$, the triply augmented basis sets are not adequately diffuse, and errors could be reduced by further augmentation of the basis set. Indeed, from the analysis of the electron density, it is clear that a sufficiently diffuse basis set would be required to represent the electron density accurately as M increases, consistent with the analysis of the CCSD total energies in Sec. IV A 1.

To quantify the deviations of the CCSD electron densities from those of the exact solutions in Fig. 1, the absolute percentage error ($|\text{PE}|$) is defined as

$$|\text{PE}| = \frac{1}{2} \int d\mathbf{r} \left| n^{\text{CCSD}}(\mathbf{r}) - n^{\text{Exact}}(\mathbf{r}) \right| \times 100\%, \quad (38)$$

where a factor of $1/2$ is included to give the absolute percentage error per electron. The results are presented in Table II, showing

TABLE II. Absolute percentage errors of CCSD electron densities estimated by Eq. (38) for the Hookium solutions with $M = 2–5$ in the t-aug-cc-pVXZ (X = D, T, Q, 5, 6) basis sets.

Orbital basis	$M = 2$ (%)	$M = 3$ (%)	$M = 4$ (%)	$M = 5$ (%)
t-aug-cc-pVDZ	13.10	17.71	21.28	14.63
t-aug-cc-pVTZ	1.59	12.57	3.51	34.73
t-aug-cc-pVQZ	3.79	8.56	3.31	31.55
t-aug-cc-pV5Z	4.27	5.99	3.97	25.76
t-aug-cc-pV6Z	3.10	2.76	3.74	20.67

that for basis sets with $X > 2$, the PEs for $M = 2$ and $M = 4$ are consistently lower than 4%. With the t-aug-cc-pV6Z basis set, CCSD calculations yield less than 4% PEs for $M = 3$. However, for $M = 5$, the PEs are greater than 20% for all t-aug-cc-pVXZ basis sets, with the exception of the t-aug-cc-pVDZ basis set. Therefore, we only consider Hookium solutions with $M = 2, 3, 4$ in the subsequent XC hole calculations using CCSD+Lieb.

B. Accuracy of finite-basis CCSD XC holes at $\lambda = 1$

We now employ the Lieb optimization at the CCSD level to compute the exchange holes at $\lambda = 0$ along with correlation holes and XC holes at $\lambda = 1$, for Hookium solutions with $M = 2, 3, 4$. The main focus of this analysis is to determine the effect of the electron–electron cusp and the limitations of finite Gaussian basis sets in its representation on the correlation hole. Moreover, we also consider the effect of the basis set size on the exchange energy E_x and correlation energy $E_c^{\lambda=1}$ for the Hookium atom solutions with $2 \leq M \leq 11$.

When comparing the CCSD $\lambda = 1$ XC holes with those of the exact solutions, the errors are dominated by the incompleteness of the finite basis set in which the orbitals are expanded. However, when comparing the CCSD $\lambda = 0$ exchange and $\lambda = 1$ correlation holes with those of the exact solutions, an additional source of error is introduced; the incompleteness of the basis set in which the potential is expanded, shown in Eq. (24), and the associated numerical errors in the convergence of the Lieb optimization at $\lambda = 0$.
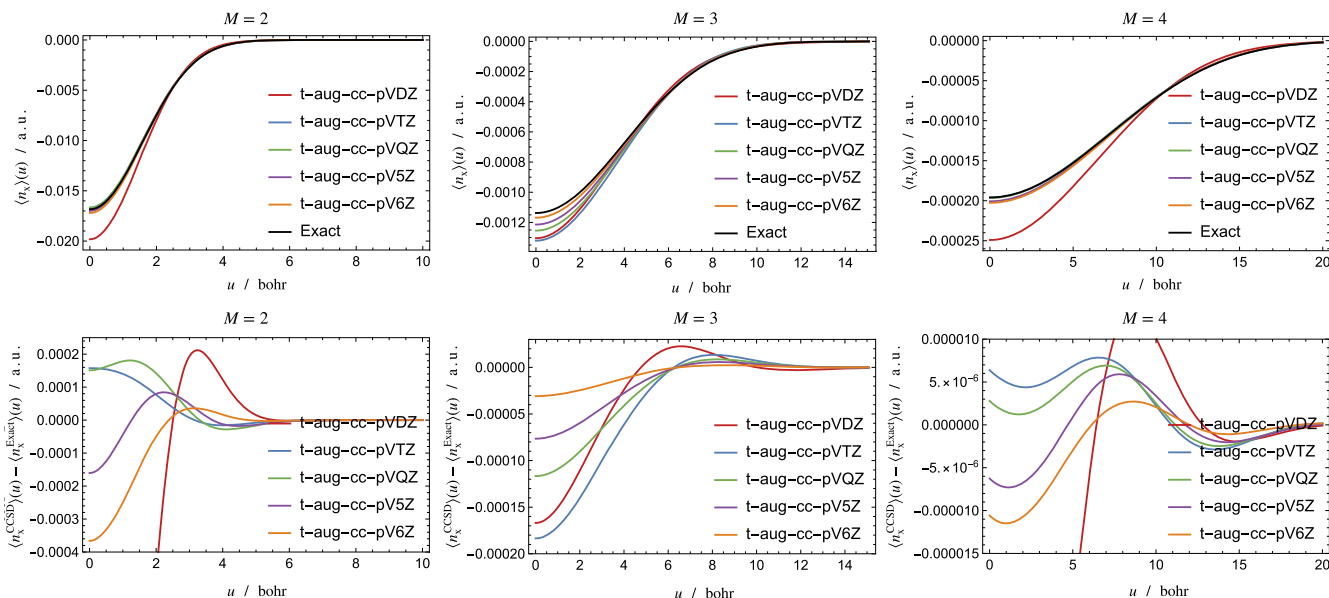
FIG. 2. System- and spherically averaged exchange holes $\langle n_x \rangle(u)$ calculated with the Lieb functional at the CCSD level for the Hookium solutions with $M = 2, 3, 4$ (upper panels) and the corresponding deviations with respect to exact results (lower panels). The orbital basis sets t-aug-cc-pVXZ with X = D, T, Q, 5, 6 are employed for each M, with corresponding potential basis sets as described in Sec. III.

1. The exchange hole

For closed-shell two-electron systems, the exchange energy is related to the Hartree energy as $E_x[n] = -\frac{1}{2}E_H[n]$, and this dominates the XC energy. In addition, the exchange hole is related to the electron density for the closed-shell two-electron system as $n_x(\mathbf{r}, \mathbf{r}') = -n(\mathbf{r}')$. As a result, the convergence of the exchange hole with respect to the basis set size is the same as that observed for the electron density. This can be seen in the upper panels of Fig. 2, Fig. 1, and Table II. Furthermore, different convergence patterns are observed in Fig. 2 for solutions of even and odd values of M. Plots of the deviation of the finite-basis exchange holes from the exact solutions in Fig. 2 indicate that basis-set convergence is generally reached with the t-aug-cc-pV6Z basis set for solutions of $M = 2, 3, 4$.

Table III presents the PEs of exchange energy E_x obtained using Lieb optimization at the CCSD level for solutions to the Hookium atom of different order M with increasing basis set size. An initial observation that can be made is that different error characteristics are again exhibited for solutions with odd and even values of M, respectively. Specifically, for $M = 2, 4$, the error is relatively small for all basis-sets with $X > 2$, while for solutions with $M = 3$ and $M = 5$, the PEs are generally larger in magnitude by comparison. Secondly, for a solution with any given M, once the number of diffuse basis functions is sufficient, increasing the cardinal number of the basis set will not increase the accuracy of the energy. For solutions with $M = 2, 3, 4$, and 5, the accuracy does not significantly improve beyond $Y = $ d, t, q, and p, respectively. For $M \geq 6$, the improvements in accuracy with increasing cardinal numbers cease at $Y = $ p.

2. The correlation hole and the description of the cusp

We now consider the system- and spherically averaged correlation holes for Hookium atoms with $M = 2, 3, 4$ in Fig. 3 and compare

them with those of the corresponding exact solutions. Figure 3 illustrates that, as the order of the Hookium solution M increases from 2 to 4, the exact correlation holes become increasingly shallow. This trend is consistent with the behavior observed in the electron densities plotted in Fig. 1 and the exchange holes in Fig. 2. In addition, the cusp at $u = 0$ becomes shallower as the order of the solution M increases, indicating that the cusp effect is less significant for more diffuse electron densities.

Figure 3 displays the effect of basis set size on the correlation holes obtained via Lieb optimization at the CCSD level. With the exception of the t-aug-cc-pV6Z basis set for the most diffuse solution with $M = 4$, enlarging the basis set results in an overall improved representation of the correlation holes with respect to those of the analytical solutions. In the lower panels of Fig. 3, the errors in the system- and spherically averaged correlation holes are plotted radially from the atomic nuclei. Compared with higher-order solutions of larger M, the maximum error for $M = 2$ arises at $u = 0$, indicating that the cusp condition is more significant the more localized the electrons are, consistent with Eq. (31). For the Hookium solution with $M = 4$, the error is more uniformly distributed radially than for solutions with $M = 2$ and $M = 3$.

To quantitatively estimate the effect of the electron–electron cusp, we define a cusp-effect driven error δE_c^{PE} in the correlation energy as

$$\delta E_c^{\text{PE}} = \frac{\int_0^{u_c} du\, 4\pi u \left[\langle n_c^{\text{CCSD}} \rangle(u) - \langle n_c^{\text{Exact}} \rangle(u) \right]}{\left| \int_0^\infty du\, 4\pi u \langle n_c^{\text{Exact}} \rangle(u) \right|} \times 100\%, \quad (39)$$

where a characteristic distance u_c defining the electron–electron cusp region is determined by the solution to

TABLE III. Percentage errors of the exchange energy E_x calculated by Lieb optimization at the CCSD level for the Hookium solutions with $M = 2$–11. Orbital basis sets of Y-aug-cc-pVXZ (X = D, T, Q, 5, 6; Y = d, t, q, p, s) and potential basis sets of (Y − 1)-aug-cc-pVXZ (X = D, T, Q, 5, 6) are employed, respectively.

Orbital basis	$M=2$	$M=3$	$M=4$	$M=5$	$M=6$	$M=7$	$M=8$	$M=9$	$M=10$	$M=11$
d-aug-cc-pVDZ	5.9%	4.1%	13.8%	70.4%	142.2%	227.0%	324.3%	434.0%	556.0%	690.1%
d-aug-cc-pVTZ	0.5%	5.9%	0.3%	43.7%	103.0%	173.7%	255.0%	346.6%	448.6%	560.7%
d-aug-cc-pVQZ	1.0%	4.0%	0.0%	41.8%	100.2%	169.7%	249.8%	340.1%	440.6%	551.1%
d-aug-cc-pV5Z	0.4%	2.7%	0.7%	42.5%	101.0%	170.8%	251.1%	341.8%	442.6%	553.5%
d-aug-cc-pV6Z	0.5%	1.0%	2.0%	44.1%	103.1%	173.6%	254.7%	346.3%	448.1%	560.2%
t-aug-cc-pVDZ	5.8%	3.0%	6.5%	5.4%	19.8%	58.4%	104.3%	156.6%	214.8%	279.1%
t-aug-cc-pVTZ	0.4%	5.3%	0.3%	5.1%	4.2%	34.5%	72.4%	116.1%	165.0%	218.9%
t-aug-cc-pVQZ	1.0%	3.6%	0.0%	5.2%	6.0%	37.1%	75.8%	120.4%	170.2%	225.3%
t-aug-cc-pV5Z	0.4%	2.3%	0.4%	5.3%	9.9%	43.0%	83.6%	130.3%	182.4%	239.9%
t-aug-cc-pV6Z	0.5%	0.8%	0.7%	4.0%	17.9%	54.7%	99.1%	149.8%	206.4%	268.8%
q-aug-cc-pVDZ	5.7%	2.8%	5.7%	4.6%	3.1%	8.7%	3.5%	25.6%	52.4%	82.7%
q-aug-cc-pVTZ	0.4%	5.2%	0.3%	5.1%	2.3%	5.7%	6.8%	8.4%	30.0%	55.1%
q-aug-cc-pVQZ	1.0%	3.5%	0.0%	5.1%	2.5%	7.3%	3.9%	13.6%	36.7%	63.4%
q-aug-cc-pV5Z	0.4%	2.3%	0.3%	4.9%	2.0%	7.9%	1.7%	22.5%	48.2%	77.4%
q-aug-cc-pV6Z	0.5%	0.8%	0.4%	3.4%	2.8%	3.4%	15.0%	41.2%	71.8%	106.1%
p-aug-cc-pVDZ	5.7%	2.8%	5.5%	4.5%	1.8%	8.0%	1.1%	5.0%	11.5%	5.2%
p-aug-cc-pVTZ	0.4%	5.2%	0.3%	5.1%	1.9%	6.2%	6.1%	1.5%	8.5%	11.7%
p-aug-cc-pVQZ	1.0%	3.5%	0.0%	5.0%	1.9%	7.3%	3.7%	1.2%	10.8%	8.7%
p-aug-cc-pV5Z	0.4%	2.3%	0.3%	4.8%	0.9%	7.3%	0.7%	6.8%	9.9%	1.6%
p-aug-cc-pV6Z	0.5%	0.8%	0.3%	3.2%	3.6%	3.4%	5.0%	8.1%	1.8%	18.1%
s-aug-cc-pVDZ	5.7%	2.8%	5.5%	4.4%	1.6%	7.9%	0.7%	6.0%	10.9%	5.1%
s-aug-cc-pVTZ	0.4%	5.2%	0.3%	5.1%	1.9%	6.3%	6.0%	0.6%	9.0%	11.0%
s-aug-cc-pVQZ	1.0%	3.5%	0.0%	5.0%	1.8%	7.3%	3.7%	2.4%	10.6%	8.0%
s-aug-cc-pV5Z	0.4%	2.2%	0.3%	4.8%	0.7%	7.2%	1.2%	7.5%	9.1%	3.3%
s-aug-cc-pV6Z	0.5%	0.8%	0.3%	3.2%	3.7%	3.5%	5.8%	7.4%	3.5%	9.5%

$$\frac{d}{du}\left[\langle n_c^{CCSD}\rangle(u) - \langle n_c^{Exact}\rangle(u)\right]\Big|_{u_c} = 0. \qquad (40)$$

Table IV presents the characteristic distance u_c and cusp-effect driven errors δE_c^{PE} computed for Hookium solutions of $M = 2, 3, 4$ with increasing basis set sizes. The trends of characteristic distances

and PEs with respect to M are in agreement with the observations in Fig. 3; solutions with higher M values exhibit smaller errors resulting from the cusp effect. This is also consistent with the cusp condition for the correlation hole expressed in Eq. (31). Since solutions of increasing M have an increasingly diffuse electron density, as shown in Fig. 1, the integral $\int dr\, n^2(\mathbf{r})/(2N)$ decreases, and $\langle n_c\rangle(0)$
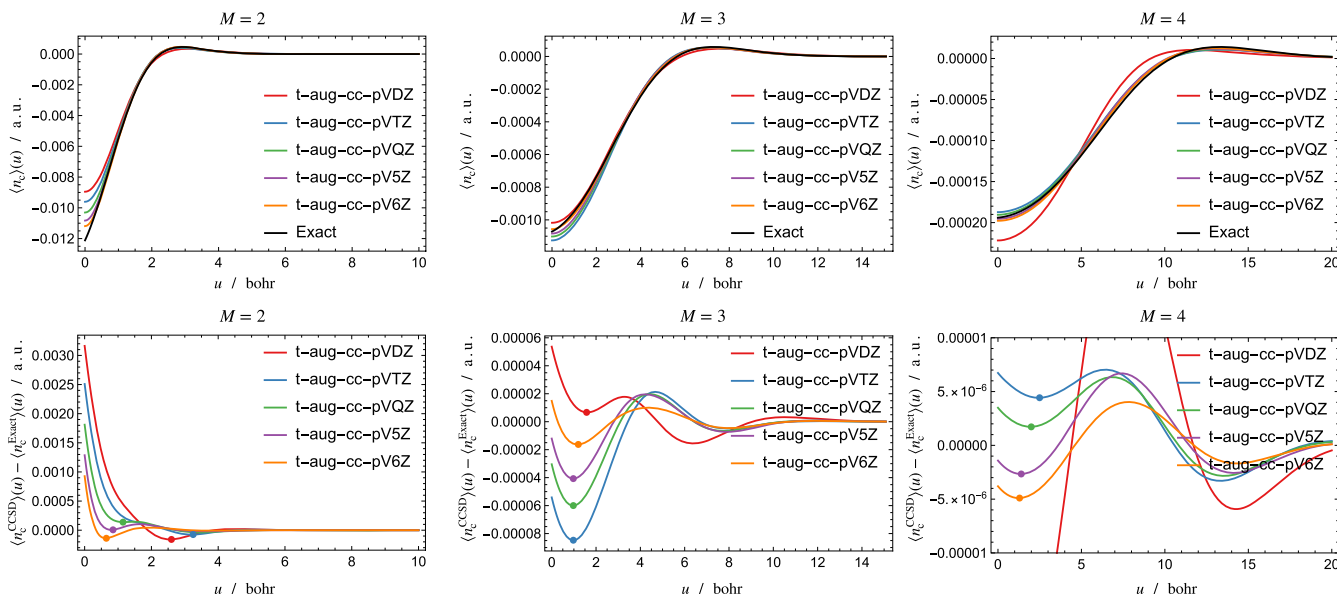
FIG. 3. System- and spherically averaged correlation hole densities $\langle n_c^{\lambda=1}\rangle(u)$ calculated by Lieb optimization at the CCSD level (upper panels) for Hookium solutions with $M = 2, 3, 4$ and corresponding errors with respect to exact results (lower panels). The colored ● indicate the characteristic distance u_c, defined in Eq. (40), associated with each basis set.

becomes smaller.[41] This, in turn, leads to a reduction in $\langle n_c'\rangle(0)$, resulting in a flatter $\langle n_c\rangle(u)$ approaching $u = 0$ for solutions of larger M, as demonstrated in Fig. 3. It follows, therefore, that the cusp-driven error becomes much less significant when M is large or the electron density is diffuse.

Table IV also shows that, as the cardinal number X of the basis set is increased from 3 to 6, the trends in u_c and δE_c^{PE} differ for each solution M. In the case of the $M = 2$ solution, it can be seen in Fig. 3 that the decrease in δE_c^{PE} with increasing X follows directly from the accompanying decrease in u_c. In contrast, for the $M = 3$ solution, the magnitude of δE_c^{PE} decreases monotonically with increasing X; however, there is no similar trend in the value of u_c, which remains constant for $3 \leq X \leq 5$ and increases for $X = 6$; instead, it can be seen

from Fig. 3 that the decrease in the magnitude of δE_c^{PE} is due to the value of $4\pi u_c\left[\langle n_c^{CCSD}\rangle(u_c) - \langle n_c^{Exact}\rangle(u_c)\right]$ decreasing as X increases, thus reducing the absolute value of the integral. For the solution with $M = 4$, the value of u_c decreases monotonically with increasing X, while the magnitude of δE_c^{PE} decreases for $3 \leq X \leq 5$ before exhibiting a small increase for $X = 6$. Fig. 3 shows that the error in the correlation hole for this solution is much less localized around $u = 0$ than for those with $M = 2$ and 3; thus, the integral from $u = 0 \rightarrow u_c$ represents a smaller area of the total integral, indicating that the cusp-driven errors δE_c^{PE} are less significant due to the diffuse electron density. The largest basis set considered in this comparison, t-aug-cc-pV6Z, yields u_c values of 0.65, 1.20, and 1.30 with corresponding cusp-driven errors δE_c^{PE} of −0.07%, −0.24%, and −0.14%

TABLE IV. The trends of the characteristic distance u_c in a.u. and cusp-effect driven errors δE_c^{PE} defined by Eqs. (40) and (39), respectively, in CCSD calculations for Hookium solutions with $M = 2, 3, 4$, with increasing basis set size.

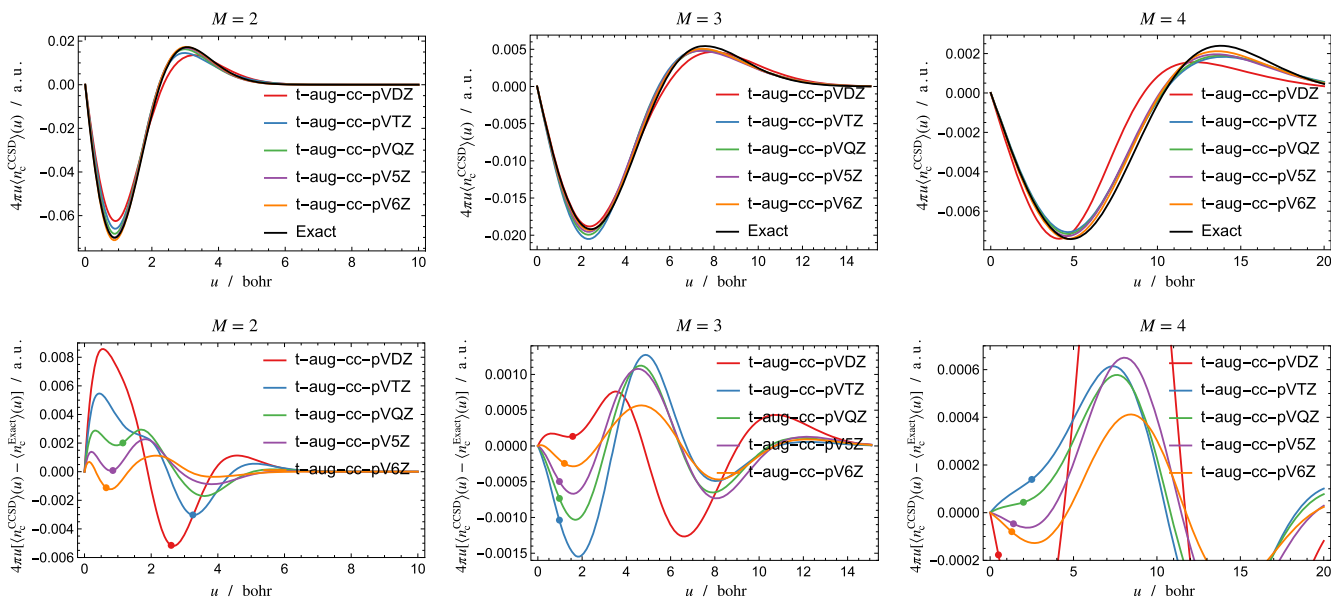|	u_c			δE_c^{PE}		
M	2	3	4	2 (%)	3 (%)	4 (%)
t-aug-cc-pVDZ	2.60	1.58	0.50	12.49	0.47	−0.13
t-aug-cc-pVTZ	3.25	0.98	2.50	9.39	−1.05	0.58
t-aug-cc-pVQZ	1.15	0.98	2.00	3.67	−0.73	0.16
t-aug-cc-pV5Z	0.85	0.98	1.40	0.87	−0.48	−0.09
t-aug-cc-pV6Z	0.65	1.20	1.30	−0.07	−0.24	−0.14

FIG. 4. CCSD evaluated $\varepsilon_c^{\lambda=1}(u) = 4\pi u \langle n_c^{\lambda=1} \rangle(u)$ (upper panels) and their differences with respect to exact results for Hookium solutions of $M = 2, 3, 4$ (lower panels). Orbital basis sets of t-aug-cc-pVXZ (X = D, T, Q, 5, 6) are employed. The colored ● indicate the characteristic distance u_c, defined in Eq. (40), associated with each basis set.

for the M = 2, 3, and 4 solutions, respectively. The remarkably small values of δE_c^{PE} exhibited by the t-aug-cc-pV6Z basis set make it an ideal reference for future investigations.

Figure 4 plots the spherically averaged correlation energy density with $\varepsilon_c^{\lambda=1}(u) = 4\pi u \langle n_c^{\lambda=1} \rangle(u)$. It shows that while the cusp-effect driven error that arises at low u is significantly attenuated at larger values of u in $\langle n_c \rangle(u)$, the error in $\varepsilon_c^{\lambda=1}(u)$ remains significant at larger values of u. Overall, calculations with the basis set with X = 6 yield a markedly improved description of $\varepsilon_c^{\lambda=1}(u)$ compared to the results obtained with smaller basis sizes for the less diffuse M = 2, 3 Hookium solutions. These observations validate the application of Lieb optimization at the CCSD level with the appropriate Gaussian basis sets to calculate XC holes accurately.

Table V collects the PEs of the correlation energy $E_c^{\lambda=1}$ calculated via Lieb optimization at the CCSD level by subtracting the Lieb $\lambda = 0$ energy from the CCSD energy. Similar trends are observed for the correlation energy with respect to Hookium atom solution M and basis set size, compared with E_x shown in Table III. While the greatest accuracy is obtained for Hookium atom solutions with $M \leq 4$, the PEs for the correlation energy are usually 3–7 times larger than those for E_x in the same calculation. For M = 2, 3, 4, the Y-aug-cc-pV6Z basis sets (Y = t, q, p, s) consistently yield accurate correlation energies with PEs of 1%–2%. However, as M increases beyond 4, the improvement in accuracy achieved by increasing the basis set size (either via larger cardinal numbers X or increased augmentation Y) is not as significant as was observed for E_x.

3. The exchange and correlation hole

Figure 5 shows the XC holes $n_{\text{xc}}^{\lambda=1}(u)$ for Hookium atom solutions with M = 2, 3, 4. The convergence of the XC holes with respect to the basis set is smoothly achieved in all three cases. In the case of M = 2, 3, the correlation components of the XC holes have significant errors due to the electron–electron cusp, and increasing the cardinal number of the basis set leads to improved accuracy. It is worth noting that for the M = 2 solution, the correlation hole around $u = 0$ from Lieb optimization at the CCSD level is too shallow, which is compensated by the X hole being too deep, with the resulting error cancellation yielding better accuracy for the XC hole than for either component individually. Overall, Lieb optimization at the CCSD level in the largest basis set, t-aug-cc-pV6Z, provides a satisfactory description of the XC hole for both the M = 2 and M = 3 Hookium atom solutions, for which the electron densities are relatively localized and not too diffuse.

C. Coupling-constant averaged XC holes and hole models

To assess the quality of the λ-averaged DFT XC holes, we first analyze how closely they align with the Lieb optimization results at the CCSD level calculated in the same basis set. This is important because CCSD-based Lieb optimizations have a much higher computational cost than DFT calculations and hence have a much greater limitation in terms of system and basis set size.

TABLE V. Absolute percentage errors of the correlation energy $E_c^{\lambda=1}$ using Lieb optimization at the CCSD level for Hookium solutions with $M = 2$–11. Orbital basis sets of Y-aug-cc-pVXZ (X = D, T, Q, 5, 6; Y = d, t, q, p, s) and potential basis sets of ($Y - 1$)-aug-cc-pVXZ (X = D, T, Q, 5, 6) are employed.

Orbital basis	$M = 2$	$M = 3$	$M = 4$	$M = 5$	$M = 6$	$M = 7$	$M = 8$	$M = 9$	$M = 10$	$M = 11$
d-aug-cc-pVDZ	5.1%	4.2%	46.1%	39.0%	22.0%	1.2%	23.1%	50.3%	80.3%	113.0%
d-aug-cc-pVTZ	7.0%	6.6%	71.8%	79.0%	75.3%	69.4%	62.2%	54.0%	44.9%	34.9%
d-aug-cc-pVQZ	6.6%	4.0%	64.2%	72.5%	67.6%	59.8%	50.2%	39.4%	27.4%	14.3%
d-aug-cc-pV5Z	4.4%	1.1%	54.4%	61.8%	54.2%	43.0%	29.4%	14.0%	3.1%	21.7%
d-aug-cc-pV6Z	1.1%	0.7%	50.7%	58.1%	49.8%	37.4%	22.5%	5.7%	13.0%	33.5%
t-aug-cc-pVDZ	5.1%	2.8%	9.8%	26.9%	25.8%	11.4%	8.2%	31.0%	56.6%	84.7%
t-aug-cc-pVTZ	6.8%	5.5%	1.9%	50.2%	84.3%	87.1%	86.0%	83.7%	80.9%	77.7%
t-aug-cc-pVQZ	6.4%	3.3%	2.8%	48.9%	80.6%	83.2%	81.5%	78.5%	74.7%	70.4%
t-aug-cc-pV5Z	4.3%	0.9%	3.8%	43.8%	69.1%	69.7%	65.4%	59.2%	51.8%	43.4%
t-aug-cc-pV6Z	1.1%	0.7%	2.0%	44.7%	61.5%	59.4%	52.4%	43.4%	32.8%	21.0%
q-aug-cc-pVDZ	5.1%	2.6%	9.7%	22.0%	20.3%	27.4%	21.8%	8.6%	7.8%	26.3%
q-aug-cc-pVTZ	6.8%	5.4%	1.6%	22.2%	1.2%	52.3%	88.8%	95.7%	95.5%	94.9%
q-aug-cc-pVQZ	6.4%	3.2%	2.2%	19.4%	2.7%	60.9%	89.4%	94.2%	94.1%	93.4%
q-aug-cc-pV5Z	4.3%	0.9%	3.0%	18.9%	6.3%	59.1%	78.0%	80.7%	79.8%	77.5%
q-aug-cc-pV6Z	1.1%	0.7%	2.2%	13.2%	20.2%	58.2%	65.9%	64.8%	60.9%	55.4%
p-aug-cc-pVDZ	5.1%	2.6%	9.8%	21.7%	21.1%	25.8%	23.9%	41.3%	37.1%	24.1%
p-aug-cc-pVTZ	6.8%	5.3%	1.5%	20.9%	0.5%	30.0%	13.5%	7.9%	60.7%	92.3%
p-aug-cc-pVQZ	6.4%	3.2%	2.2%	18.0%	2.0%	25.5%	12.3%	29.7%	79.9%	99.5%
p-aug-cc-pV5Z	4.3%	0.9%	2.9%	17.3%	5.0%	24.7%	10.7%	47.0%	77.9%	89.1%
p-aug-cc-pV6Z	1.1%	0.7%	2.3%	11.7%	16.8%	11.9%	25.7%	58.2%	68.9%	70.6%
s-aug-cc-pVDZ	5.1%	2.6%	9.8%	21.6%	21.3%	25.5%	24.7%	41.1%	35.6%	24.6%
s-aug-cc-pVTZ	6.8%	5.3%	1.5%	20.7%	0.3%	28.8%	13.0%	9.6%	39.3%	28.2%
s-aug-cc-pVQZ	6.4%	3.2%	2.2%	17.8%	2.1%	24.2%	10.4%	21.2%	30.1%	23.3%
s-aug-cc-pV5Z	4.3%	0.8%	2.9%	17.1%	5.2%	22.8%	7.1%	30.5%	28.5%	18.9%
s-aug-cc-pV6Z	1.1%	0.7%	2.3%	11.5%	16.5%	11.1%	23.0%	22.8%	13.0%	41.4%

In Fig. 6, we have plotted the accuracy of LDA hole densities evaluated by $\langle n_x^{\text{LDA}} \rangle(u) - \langle n_x^{\text{CCSD}} \rangle(u)$, $\langle \bar{n}_c^{\text{LDA}} \rangle(u) - \langle \bar{n}_c^{\text{CCSD}} \rangle(u)$, and $\langle \bar{n}_{xc}^{\text{LDA}} \rangle(u) - \langle \bar{n}_{xc}^{\text{CCSD}} \rangle(u)$. The cardinal number X of the basis set was increased continuously from 2 to 6 to examine the convergence of this error with respect to the basis set size. It is important to note that the errors corresponding to the $X = 2$ basis set show a different behavior from those of the larger basis sets, indicating that this small basis is typically insufficient to accurately evaluate the λ-averaged XC holes. This is consistent with the previous discussion concerning the $\lambda = 1$ case.

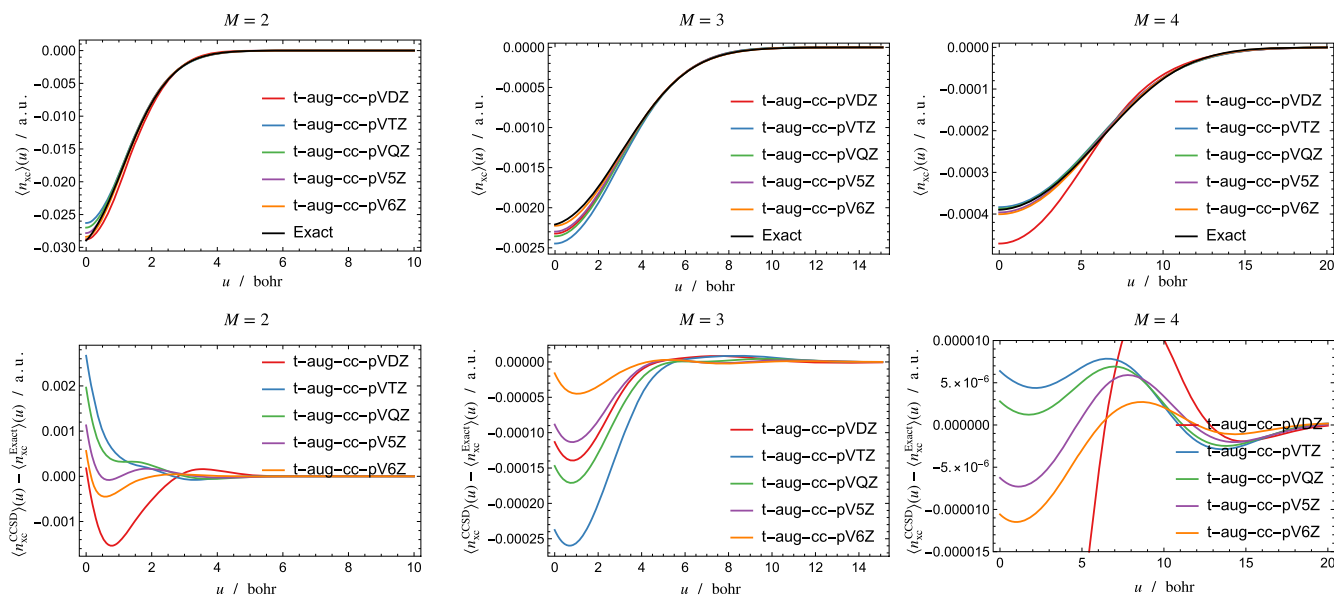24 January 2024 15:35:23

FIG. 5. The system- and spherically averaged XC hole density $\langle n_{xc}^{\lambda=1}\rangle(u)$ calculated at the CCSD level (upper panels) for Hookium solutions with $M = 2, 3, 4$ in the t-aug-cc-pVXZ ($X = $ D, T, Q, 5, 6) orbital basis sets, and the deviations with respect to those of the analytical solutions (lower panels).

Figure 6 shows that the largest change in $\langle n_{x}^{LDA}\rangle(u)$ $- \langle n_{x}^{CCSD}\rangle(u)$ with respect to the basis set size occurs at the value of u with the largest error, particularly in the case of the $M = 3$ Hookium atom solution. Nevertheless, overall, the LDA hole model calculations of the exchange holes exhibit rapid convergence in their errors with respect to basis set size, suggesting that the accuracy of the DFT exchange holes is relatively insensitive to basis set size.

However, for the λ-averaged correlation holes, the situation is somewhat different. Changes in the error of the LDA correlation holes with respect to increasing basis set size are most visible around the first peak in the radial plots of the correlation holes, extending to subsequent peaks further from the nucleus for the $M = 3, 4$ Hookium atom solutions. As the basis set grows, the position of the first peak tends to shift toward $u = 0$. This could be attributed to the fact that the cusp-driven deviations become less significant with larger basis sets with CCSD-based calculations, whereas LDA satisfies the cusp condition and converges much more rapidly with basis set size.

Although the exchange hole is the dominant component of the XC hole, the errors of the LDA exchange holes and correlation holes are comparable in size. In Fig. 6, the errors at short-range for the LDA XC holes are dominated by the correlation hole contribution, while errors at mid-range mainly arise from the LDA exchange hole or both. Overall, accurate λ-averaged XC hole (or correlation hole) calculations require the use of basis-sets with $X \geq 4$. It is worth mentioning that similar trends are observed for the PBE hole model, the results of which are presented in the supplementary material.

The XC holes obtained with different basis sets are used to calculate the corresponding LDA XC energies, and Table VI presents

the PEs of the LDA XC energies relative to Lieb optimization values at the CCSD level for basis sets of increasing size. Table VI shows that the PE variations of the LDA exchange energy are relatively small, within 0.2%, while the convergence behavior of correlation energy for the Hookium solutions with $M = 3, 4$ exhibits no clear trend. However, for the $M = 2$ solution, in which the cusp-effect driven error is the most significant in the CCSD calculations, the PE changes of the LDA correlation energy with increasing basis set size are slightly larger. The changes in the PE of E_{xc} with increasing basis-set size are similar to that of the exchange energy, with only a change of 0.3% for the $M = 2$ solution from the smallest to the largest basis set; this is because E_{x} represents the vast majority of E_{xc}.

In Fig. 7, the exchange holes, λ-averaged correlation holes, and XC holes from the LDA hole model, PBE hole model, and Lieb optimizations at the CCSD level are presented with the t-aug-cc-pV6Z basis set. Figure 7 shows that both the LDA and PBE hole models, in particular the LDA one, tend to localize the exchange hole, regardless of the order of the solution M. For the correlation holes, although both LDA and PBE hole models capture the cusp condition, they exhibit almost linear behavior before reaching their maximum value, resulting in an overly shallow correlation hole density in the small u region but an overly deep correlation hole at the intermediate u region. Figure 7 also shows that, for both the exchange and correlation holes, the PBE hole model is superior to the corresponding LDA hole model. However, the LDA and PBE model XC holes appear much more similar due to error cancellation between their respective X and C holes.
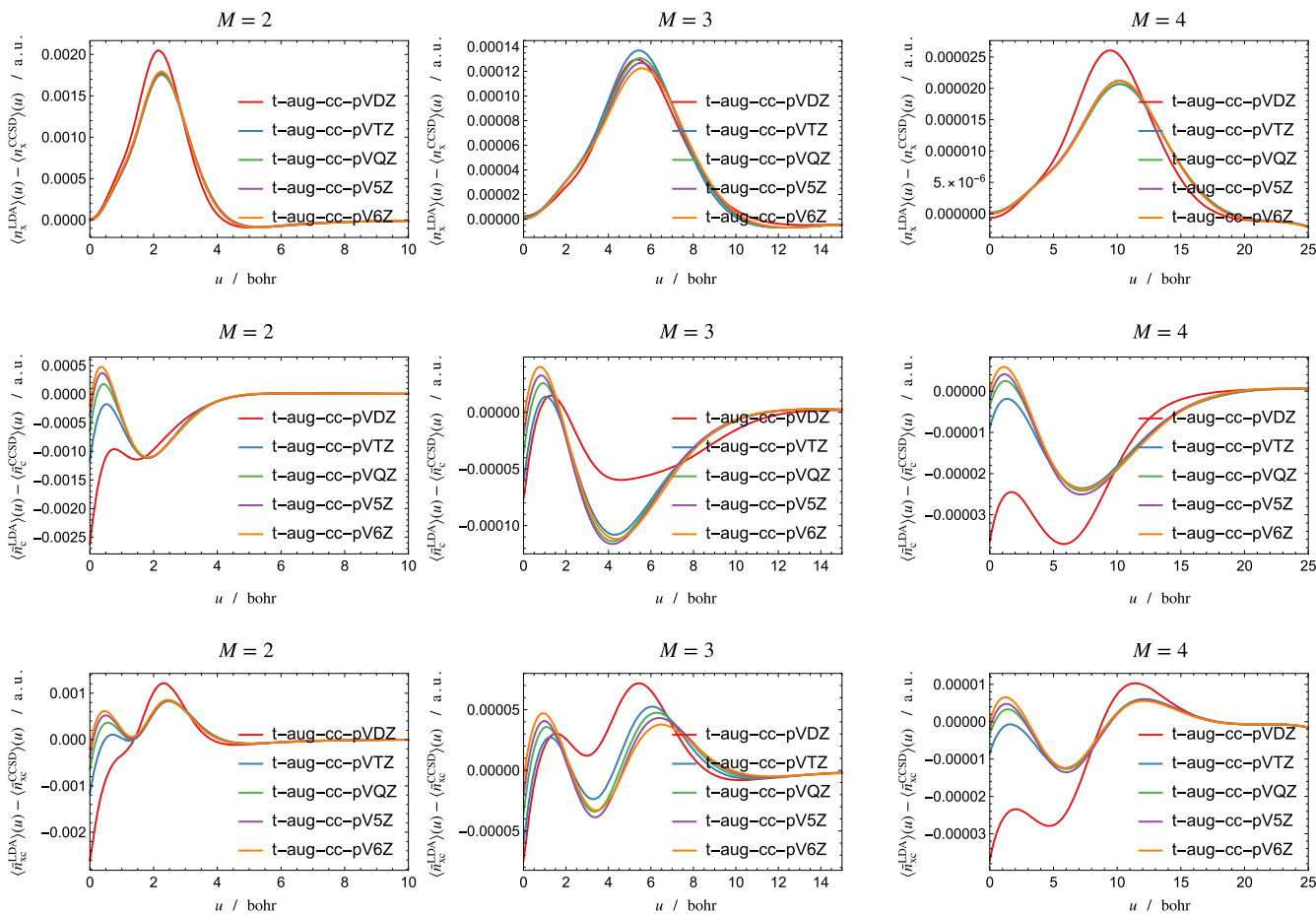
FIG. 6. Deviations of LDA hole densities $\langle n_x^{LDA} \rangle(u)$, $\langle \bar{n}_c^{LDA} \rangle(u)$ and $\langle \bar{n}_{xc}^{LDA} \rangle(u)$ from the corresponding Lieb optimization results at the CCSD level employing the same basis set for Hookium solutions with $M = 2, 3, 4$.

TABLE VI. Percentage errors of energy components E_x^{LDA}, E_c^{LDA}, and E_{xc}^{LDA} calculated from the LDA hole model relative to the CCSD+Lieb results under the same orbital basis set for Hookium solutions of $M = 2, 3, 4$.

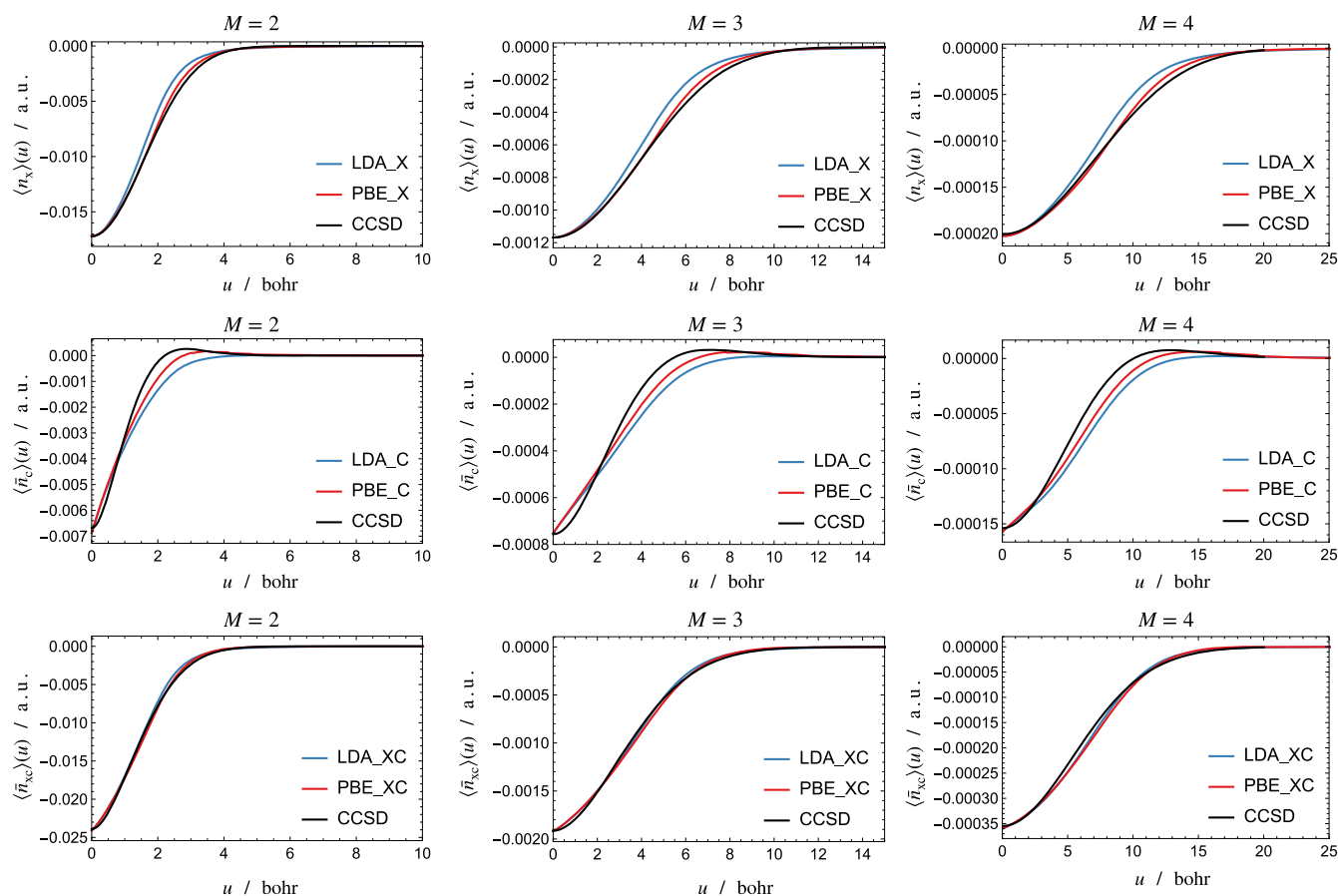|	E_x^{LDA}			E_c^{LDA}			E_{xc}^{LDA}		
M	2 (%)	3 (%)	4 (%)	2 (%)	3 (%)	4 (%)	2 (%)	3 (%)	4 (%)
t–aug–cc–pVDZ	14.4	14.6	14.9	−155.4	−63.1	−107.9	4.2	3.9	−1.8
t–aug–cc–pVTZ	14.5	14.2	14.9	−146.0	−83.8	−79.2	4.3	2.2	−0.1
t–aug–cc–pVQZ	14.6	14.3	14.9	−138.7	−88.6	−78.6	4.5	1.8	−0.1
t–aug–cc–pV5Z	14.6	14.3	14.8	−132.1	−92.2	−79.9	4.7	1.6	−0.2
t–aug–cc–pV6Z	14.5	14.4	14.7	−126.5	−92.3	−76.8	4.8	1.5	0.0

FIG. 7. System- and spherical-averaged $\langle n_x \rangle(u)$, and λ-averaged $\langle \bar{n}_c \rangle(u)$, $\langle \bar{n}_{xc} \rangle(u)$ calculated by LDA and PBE hole models as compared with the Lieb optimization results at the CCSD level for Hookium solutions with $M = 2, 3, 4$ in the t-aug-cc-pV6Z orbital basis set and d-aug-cc-pV6Z potential basis set.

V. CONCLUSION

In this study, we have employed the Lieb optimization approach with CCSD used as the reference wave function method to obtain accurate representations of the XC hole of the Hookium atom—a model system for which exact solutions can be obtained. Our investigation focuses on the difficulty in representing the electron–electron cusp condition within a finite Gaussian basis set, the manifestation of this in the correlation hole, and the effect on the cusp-related error of increasing the basis set size. We have found that the error resulting from the cusp effect can be effectively and sufficiently reduced by using a larger basis set and that the cusp condition in the correlation hole becomes less significant for larger M Hookium atom solutions with diffuse electron densities. For smaller M Hookium solutions with electron densities that are more localized, the coupling-constant-averaged XC holes were calculated using the Lieb optimization with a CCSD reference wave function and used as a reference to benchmark DFT XC hole models. We confirmed the presence of significant error cancellation between the exchange hole and correlation hole for both PBE and LDA hole models, and this results in their XC holes having greater accuracy than either the exchange or correlation holes alone.

In this work, we focused on a limited number of cases for which exact solutions are available as a benchmark. These solutions correspond to relatively low confinement as M increases. However, solutions can be obtained using numerical grid based procedures for general confinements with very high accuracy (see, for example, Refs. 42 and 43). In the future, benchmarks could be generated using a numerical approach for stronger confinement, allowing a study of the cusp-driven errors in more compact densities closer to those in real atoms and molecules. Standard Gaussian basis sets were employed throughout this study, leading to some limitations in the accuracy to which benchmark quantities could be reproduced. In the future, basis-set optimization could be carried out to further refine the agreement with the benchmark solutions.

A significant advantage of the present implementation is its flexibility, which opens up several possibilities for further work. The approach presented can be readily applied to cases with $N > 2$, for which benchmark data are available.[44] The range of interaction strengths, λ, to be considered could also be extended and compared

24 January 2024 15:35:23

with the strong interaction limit. With very minor modifications, interactions other than the Coulomb potential could be considered (see, for example, recent work on erfonium).[45]

In general, the apparatus presented in this work allows for the Lieb functional, adiabatic connection, and exchange–correlation holes to be studied for model systems where (near) exact solutions can be readily obtained for the physical system ($\lambda = 1$). Furthermore, these solutions can be smoothly connected to the corresponding Kohn–Sham auxiliary system ($\lambda = 0$). Given that these benchmark model systems play a central role in the development and testing of new density functional approximations, we expect that the tools presented in this work will be useful in this context.

SUPPLEMENTARY MATERIAL

Comparisons between the PBE XC hole model and the CCSD coupling-constant averaged XC holes are presented in the supplementary material. See Sec. IV C for discussion of these quantities.

AUTHOR DECLARATIONS

Conflict of Interest

The authors have no conflicts to disclose.

Author Contributions

Lin Hou: Formal analysis (equal); Investigation (equal); Writing – original draft (equal). **Tom J. P. Irons**: Conceptualization (equal); Formal analysis (equal); Investigation (equal); Methodology (equal); Software (equal); Supervision (equal); Writing – original draft (equal); Writing – review & editing (equal). **Yanyong Wang**: Investigation (equal); Supervision (equal); Writing – original draft (equal). **James W. Furness**: Formal analysis (equal); Investigation (equal); Software (equal). **Andrew M. Wibowo-Teale**: Conceptualization (equal); Formal analysis (equal); Funding acquisition (equal); Investigation (equal); Methodology (equal); Software (equal); Supervision (equal); Writing – review & editing (equal). **Jianwei Sun**: Conceptualization (equal); Formal analysis (equal); Funding acquisition (equal); Investigation (equal); Methodology (equal); Project administration (equal); Supervision (equal); Writing – review & editing (equal).

DATA AVAILABILITY

The data that supports the findings of this study are available within the article and its supplementary material.

APPENDIX: REFERENCE POTENTIAL USED IN THE LIEB OPTIMIZATION

In this work, the reference potential employed in the Lieb optimization is a modified form of the localized Hartree–Fock potential,[24] in which the Slater non-local exchange potential is corrected at long-range by an approximate Fukui potential[25] to avoid the numerical instabilities associated with calculating the Slater potential at low densities. In terms of spin-σ Kohn–Sham orbitals $\psi_{i\sigma}$, the Slater exchange potential v_{Sx}^σ and approximate Fukui potential v_{f}^σ are given, respectively, by

$$v_{\text{Sx}}^\sigma(\mathbf{r}) = -\frac{1}{n_\sigma(\mathbf{r})} \sum_{ij}^{occ} \psi_{i\sigma}^*(\mathbf{r})\psi_{j\sigma}(\mathbf{r}) \int d\mathbf{r}' \frac{\psi_{i\sigma}^*(\mathbf{r}')\psi_{j\sigma}(\mathbf{r}')}{|\mathbf{r} - \mathbf{r}'|}, \quad (A1)$$

$$v_{\text{f}}^\sigma(\mathbf{r}) = -\int d\mathbf{r}' \frac{|\psi_{\text{HOMO}\sigma}(\mathbf{r}')|^2}{|\mathbf{r} - \mathbf{r}'|}. \quad (A2)$$

Due to the division by density in Eq. (A1), the Slater potential becomes numerically unstable to calculate in asymptotic regions where the density is very small; however, the Fukui potential can be evaluated in these regions without numerical instability. In this work, the reference exchange potential is constructed from a density-dependent admixture of Slater and Fukui potentials as

$$v_{\text{ref,x}}^\sigma(\mathbf{r}) = \kappa_\sigma(\mathbf{r})v_{\text{Sx}}^\sigma(\mathbf{r}) + (1 - \kappa_\sigma(\mathbf{r}))v_{\text{f}}^\sigma(\mathbf{r}),$$
$$\kappa_\sigma(\mathbf{r}) = \frac{n_\sigma(\mathbf{r})}{\eta + n_\sigma(\mathbf{r})}, \quad (A3)$$

where the parameter η is selected to determine the density at which the reference potential is an equal mixture of Slater and Fukui potentials—here, a value of $\eta = 2 \times 10^{-6}$ a.u. is used. The potential in Eq. (A3) is used in place of the Slater potential in the calculation of the localized Hartree–Fock potential, which applies a further correction to better reproduce the exact exchange potential. The resulting potential is then used as the reference potential in the Lieb optimization.

REFERENCES

[1] P. Hohenberg and W. Kohn, "Inhomogeneous electron gas," Phys. Rev. **136**, B864–B871 (1964).

[2] W. Kohn and L. J. Sham, "Self-consistent equations including exchange and correlation effects," Phys. Rev. **140**, A1133–A1138 (1965).

[3] R. Parr and W. Yang, *Density-Functional Theory of Atoms and Molecules* (Oxford University Press, New York, 1989).

[4] J. P. Perdew and S. Kurth, "Density functionals for non-relativistic Coulomb systems in the new century," in *A Primer in Density Functional Theory*, edited by C. Fiolhais, F. Nogueira, and M. Marques (Springer Berlin Heidelberg, 2003), pp. 1–55.

[5] J. P. Perdew, J. A. Chevary, S. H. Vosko, K. A. Jackson, M. R. Pederson, D. J. Singh, and C. Fiolhais, "Atoms, molecules, solids, and surfaces: Applications of the generalized gradient approximation for exchange and correlation," Phys. Rev. B **46**, 6671–6687 (1992).

[6] J. Sun, A. Ruzsinszky, and J. P. Perdew, "Strongly constrained and appropriately normed semilocal density functional," Phys. Rev. Lett. **115**, 036402 (2015).

[7] R. J. McCarty, D. Perchak, R. Pederson, R. Evans, Y. Qiu, S. R. White, and K. Burke, "Bypassing the energy functional in density functional theory: Direct calculation of electronic energies from conditional probability densities," Phys. Rev. Lett. **125**, 266401 (2020).

[8] Q. Wu and W. Yang, "A direct optimization method for calculating density functionals and exchange–correlation potentials from electron densities," J. Chem. Phys. **118**, 2498–2509 (2003).

[9] E. H. Lieb, "Density functionals for Coulomb systems," Int. J. Quantum Chem. **24**, 243–277 (1983).

[10] A. M. Teale, S. Coriani, and T. Helgaker, "The calculation of adiabatic-connection curves from full configuration-interaction densities: Two-electron systems," J. Chem. Phys. **130**, 104111 (2009).

[11] A. M. Teale, S. Coriani, and T. Helgaker, "Accurate calculation and modeling of the adiabatic connection in density functional theory," J. Chem. Phys. **132**, 164115 (2010).

[12] J. Kimball, "Short-range correlations and electron-gas response functions," Phys. Rev. A **7**, 1648 (1973).

[13] E. R. Davidson, *Reduced Density Matrices in Quantum Chemistry* (Academic Press, New York, 1976).

[14] K. Burke and J. P. Perdew, "Real-space analysis of the exchange-correlation energy," Int. J. Quantum Chem. **56**, 199–210 (1995).

[15] H. Luo and A. Alavi, "Combining the transcorrelated method with full configuration interaction quantum Monte Carlo: Application to the homogeneous electron gas," J. Chem. Theory Comput. **14**, 1403–1411 (2018).

[16] M. Taut, "Two electrons in an external oscillator potential: Particular analytic solutions of a Coulomb correlation problem," Phys. Rev. A **48**, 3561 (1993).

[17] S. Kais, D. Herschbach, N. Handy, C. Murray, and G. Laming, "Density functionals and dimensional renormalization for an exactly solvable model," J. Chem. Phys. **99**, 417–425 (1993).

[18] D. Langreth and J. Perdew, "The exchange-correlation energy of a metallic surface," Solid State Commun. **17**, 1425–1429 (1975).

[19] R. McWeeny, "Some recent advances in density matrix theory," Rev. Mod. Phys. **32**, 335–369 (1960).

[20] P. E. Lammert, "Differentiability of Lieb functional in electronic density functional theory," Int. J. Quantum Chem. **107**, 1943 (2007).

[21] S. Kvaal, U. Ekström, A. M. Teale, and T. Helgaker, "Differentiable but exact formulation of density-functional theory," J. Chem. Phys. **140**, 18A518 (2014).

[22] T. Heaton-Burgess, F. A. Bulat, and W. Yang, "Optimized effective potentials in finite basis sets," Phys. Rev. Lett. **98**, 256401 (2007).

[23] W. Yang and Q. Wu, "Direct method for optimized effective potentials in density-functional theory," Phys. Rev. Lett. **89**, 143002 (2002).

[24] F. Della Sala and A. Görling, "Efficient localized Hartree–Fock methods as effective exact-exchange Kohn–Sham methods for molecules," J. Chem. Phys. **115**, 5718–5732 (2001).

[25] R. G. Parr and W. Yang, "Density functional approach to the frontier-electron theory of chemical reactivity," J. Am. Chem. Soc. **106**, 4049–4050 (1984).

[26] See https://quest.codes/ for "QUEST, a rapid development platform for QUantum electronic structure techniques."

[27] Q. Wu and W. Yang, "Algebraic equation and iterative optimization for the optimized effective potential in density functional theory," J. Theor. Comput. Chem. **02**, 627–638 (2003).

[28] C. R. Myers, C. J. Umrigar, J. P. Sethna, and J. D. Morgan, "Fock's expansion, Kato's cusp conditions, and the exponential ansatz," Phys. Rev. A **44**, 5537–5546 (1991).

[29] K. Burke, J. P. Perdew, and M. Ernzerhof, "Why semilocal functionals work: Accuracy of the on-top pair density and importance of system averaging," J. Chem. Phys. **109**, 3760–3771 (1998).

[30] Z. Qian and V. Sahni, "Physics of transformation from Schrödinger theory to Kohn-Sham density-functional theory: Application to an exactly solvable model," Phys. Rev. A **57**, 2527 (1998).

[31] L. A. Constantin, E. Fabiano, and F. Della Sala, "Construction of a general semilocal exchange-correlation hole model: Application to nonempirical meta-GGA functionals," Phys. Rev. B **88**, 125112 (2013).

[32] K. Burke, J. Angulo, and J. P. Perdew, "Validity of the extended electron-electron cusp condition," Phys. Rev. A **50**, 297 (1994).

[33] K. Burke, J. P. Perdew, and D. C. Langreth, "Is the local density approximation exact for short wavelength fluctuations?," Phys. Rev. Lett. **73**, 1283 (1994).

[34] T. H. Dunning, "Gaussian basis sets for use in correlated molecular calculations. I. The atoms boron through neon and hydrogen," J. Chem. Phys. **90**, 1007–1023 (1989).

[35] D. E. Woon and T. H. Dunning, "Gaussian basis sets for use in correlated molecular calculations. III. The atoms aluminum through argon," J. Chem. Phys. **98**, 1358–1371 (1993).

[36] D. E. Woon and T. H. Dunning, "Gaussian basis sets for use in correlated molecular calculations. V. Core-valence basis sets for boron through neon," J. Chem. Phys. **103**, 4572–4585 (1995).

[37] V. Lebedev, "Quadratures on a sphere," USSR Comput. Math. Math. Phys. **16**, 10–24 (1976).

[38] V. I. Lebedev and A. L. Skorokhodov, "Quadrature formulas for a sphere of orders 41, 47 and 53," Dokl. Akad. Nauk SSSR **324**, 519–524 (1992).

[39] R. Lindh, P.-Å. Malmqvist, and L. Gagliardi, "Molecular integrals by numerical quadrature. I. radial integration," Theor. Chem. Acc. **106**, 178–187 (2001).

[40] *Mathematica, version 13.3*, Wolfram Research, Inc., Champaign, IL, 2023.

[41] J. P. Perdew and Y. Wang, "Pair-distribution function and its coupling-constant average for the spin-polarized electron gas," Phys. Rev. B **46**, 12947 (1992).

[42] J. Karwowski and A. Savin, "Two-particle coalescence conditions revisited," Mol. Phys. **120**, e2069055 (2022).

[43] J. Karwowski and A. Savin, "Erfonium: A Hooke atom with soft interaction potential," in *Advances in Methods and Applications of Quantum Systems in Chemistry, Physics, and Biology: Selected Proceedings of QSCP-XXV Conference (Toruń, Poland, June 2022)* (in press); arXiv:2308.12717 (2023).

[44] J. Cioslowski and K. Strasburger, "Five- and six-electron harmonium atoms: Highly accurate electronic properties and their application to benchmarking of approximate 1-matrix functionals," J. Chem. Phys. **148**, 144107 (2018).

[45] A. Savin and J. Karwowski, "Correcting models with long-range electron interaction using generalized cusp conditions," J. Phys. Chem. A **127**, 1377–1385 (2023).